Semiconductor Junction Gas Sensors

Karin Potje-Kamloth

Chem. Rev., **2008**, 108 (2), 367-399 • DOI: 10.1021/cr0681086

Semiconductor Junction Gas Sensors

Karin Potje-Kamloth*

Institut fuer Mikrotechnik Mainz, Carl-Zeiss-Strasse 18-20, 55129 Mainz, Germany

Received July 11, 2007

Contents

1. Introduction

Over the past three decades, a number of studies have been undertaken to characterize the interactions of gases and chemical species with semiconductors as well as to develop useful sensing devices based on these effects.[1] Examples include gas detectors using metal-oxide semiconductor field-effect transistors,[2−4] metal-oxide semiconductor capacitors,[5] as well as Schottky barrier diodes.[6] Among those, Schottky barrier diode sensors are devices which are extremely simple to fabricate, obviating the need for photolithography or high-temperature diffusion/oxidation steps. These sensors may be broadly classified into two categories: (1) *interface-controlled devices*, in which the species of interest are adsorbed at the metal surface and thus affect interfacial polarization, and (2) *bulk-controlled devices*, which are dependent on the change in bulk properties of the semiconductor caused by absorption of and interaction with the diffusing species.

Schottky barrier based gas sensors have been fabricated with a number of inorganic semiconductors using catalytic metals as the metal contact,[6−11] mostly for detection of hydrogen. Due to various hydrogen-induced changes in catalytic metals, the change of the interface properties of the Schottky barrier diode readily lends itself to applications in interface-controlled sensors devices.[6] The metal/inorganic semiconductor Schottky diodes can exhibit a very high sensitivity and low detection limit to hydrogen. The success of these devices translates into a huge number of papers published on the subject of hydrogen sensing. Unfortunately, the range of applicability is limited to the detection of hydrogen and hydrogen-producing gases or vapors, which comes from the exclusive solubility and permeability of atomic hydrogen in such materials.

This limitation does not apply to the class of organic semiconductors, which includes organic molecules as well

* E-mail: potje@imm-mainz.de.

10.1021/cr0681086 CCC: $71.00
Published on Web 01/30/2008

Karin Potje-Kamloth studied chemistry at Ludwigs Maximilians Universität München and received her Ph.D. and Habilitation in physical chemistry. Currently, she is a senior scientist at Institut fuer Mikrotechnik Mainz GmbH. Her main research areas of interest are low cost chemical sensors, thin film technology of advanced polymer materials, energy harvesting, and chemical sensing platforms for microsystems

as conjugated polymers. They show almost unlimited permeability for gases and vapors, and the concomitant ability to form charge-transfer complexes with the matrix. Moreover, they offer the possibility to tune the sensitivity and selectivity toward gases and vapors by chemical alternation of the polymer backbone, addition of side groups, alternation of the lengths of the polymer chain, and alternation of the nature of the dopant. Variations in the chemical and physical properties of the organic semiconductors are manifold and represent a further advantage for organic semiconductors in this application area. For this reason, the focus of this review is on the progress in metal/organic semiconductor based Schottky barrier junction sensors.

The use of organic semiconducting materials has received considerable interest as the active component in electronic device structures,[12−18] such as organic light emitting diodes (OLEDs),[19,20] solar cells,[21,22] and organic field-effect transistors,[23,24] Schottky diodes,[25] and gas sensors.[26−30] In the case of field-effect transistors (FETs), the organic semiconductor can either be the active component, i.e., the current carrying material, of the organic FET (OFET) or the selective layer used as the gate electrode in a chemical sensitive FET (CHEMFET). The interaction of gases or vapors with the bulk of organic semiconductors affects the work function of the organic semiconductor, which modifies the electrical properties of the electronic device. This leads to the application of organic semiconductors in bulk-controlled devices.

The metal/semiconductor interface is the obvious component in any semiconductor device and controls the Schottky barrier device characteristic. The theoretical aspects of interfaces in devices based on organic semiconductors closely resemble those of inorganic ones. This allows in general the use of the extensive knowledge accumulated during many years of studies of the electronic properties of inorganic semiconductors.

The purpose of this review is to introduce the reader to the field of metal/semiconductor junctions, in particular metal/organic semiconductor junctions, by providing insights into some of the theoretical and experimental approaches that have been employed thus far, although it is not meant to be an exhaustive study of all of the research work and techniques employed in the study of interface formation in semiconductor devices. This topic is too broad and is beyond the scope of this review.

The second section gives an introduction to the physics of organic semiconductors, which are relevant to the understanding of the peculiar properties of interfaces in organic semiconductor devices. The third section deals with some theoretical aspects concerning metal/semiconductor junctions and their use in chemical sensing. The fourth section is a review of this area of semiconductor junction gas sensors and deals with the electrical and gas sensing properties of Schottky barrier diodes. Both sections cover inorganic and organic semiconductor Schottky barrier diodes. Furthermore, section 4 shows how experimental and structural parameters of semiconductors can influence the Schottky barrier junction and hence the diode characteristics. The reader who is familiar with organic semiconductor polymers and the electrical properties of semiconductor contacts can skip directly to section 4, and those interested in an overview of this class of materials and of these types of devices may find sections 2 and 3 to be useful.

2. Properties of Organic Semiconductors

The word “organic semiconductors” includes polymers and low-molecular-weight organic materials. The former are usually characterized by ill-defined chain lengths while the latter show both a well-defined composition and length. The use of the name “*organic semiconductor*” is based on the extrinsic semiconducting properties of organic systems, i.e., the capacity to transport charge generated by light, injected by electrodes, or provided by chemical dopants. Due to the weak electronic coupling between organic molecules, disorder plays a central role in the understanding of these materials. Disorder manifests itself in varying the energy levels of the electronic states of different molecules and the structure of the solid state. Both strongly influence the transport mechanism of charge carriers and charge injection at metal/semiconductor interfaces.

2.1. Electronic Properties of Organic Semiconductors

2.1.1. Molecular Semiconductors

In inorganic semiconductor crystals such as silicon or germanium, the strong coupling between the atoms and the long-range order lead to the delocalization of the electronic states and the formation of allowed valence and conduction bands, separated by a forbidden energy gap. By thermal activation or photoexcitation, free electrons are generated in the conduction band, leaving behind positively charged holes in the valence band. The transport of these free charge carriers is described in the quantum mechanical language of Bloch functions, k-space, and dispersion relations familiar to solid-state physicists.[31]

In organic solids, intramolecular interactions are mainly covalent, but intermolecular interactions are due to much weaker van der Waals and London forces. As a result, the transport bands in organic crystals are much narrower than those of their inorganic counterparts and the band structure is easily disrupted by introducing disorder in the system. Thus, even in molecular crystals, the concept of allowed energy bands is of limited validity and excitations as well as interactions localized on individual molecules play a predominant role. The common electronic feature of molecular semiconductors is the π-conjugated system, which is formed by the overlap of carbon p_z-orbitals. In Figure 1 the

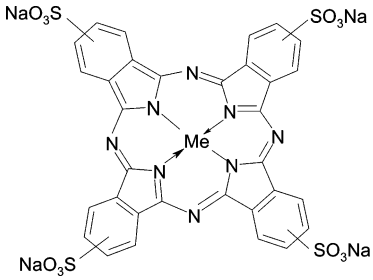

Figure 1. Molecular structure of metallophthalocyanine tetrasulfonate (MPcTS) salt.

molecular structure of a typical representative of this class of semiconductors, metallophthalocyanine tetrasulfonate (MPcTS), is shown. The orbital system of the ring comprises 42 π-electrons. Due to the orbital overlap, the π-electrons are delocalized within the molecule and the energy gap between the highest occupied molecular orbital (HOMO) and the lowest unoccupied molecular orbital (LUMO) is small, i.e., exhibiting transition frequencies within the visible range.

Activation of free electrons by photoexcitation or chemical doping can lead to a tremendous increase of the electric conductivity from about 10^{-12} S cm^{-1} to values in the range of 10^{2} S cm^{-1}, which indicates the semiconducting character of the material.

2.1.2. Conducting Polymers

Polymers are typically associated with flexible, processible materials having electrically insulating properties. Although this is true of most polymers, a special class of these materials called conjugated polymers has the electrical and optical properties traditionally associated with metals and semiconductors, yet they retain the mechanical properties and the processability of plastics.

Conjugated polymers are characterized by repeated units in which atomic valence is not satisfied by covalent bonds. The leftover valence electrons of adjacent carbon atoms overlap and form double bonds that give rise to π-bonds, in which the π-electrons are delocalized over large segments of the polymer chain. They are forming the so-called π-conjugated system, which is responsible for the electronic properties of the conjugated polymers. The chemical structures of the most thoroughly studied conducting polymers are shown in Figure 2.

Polymers can consist of on the order of 10^{5} to 10^{6} (or even a greater number) monomers strung together to form a macromolecular chain. Typical conjugated polymers include straight chain units, five or six-membered rings, and all combinations of these. The addition of heteroatoms (atoms other than carbon and hydrogen) and side chains allows for an even larger variety in this class. Their electronic properties can be tailored by the synthesis, and their electrical conductivity can be varied from about 10^{-12} S cm^{-1} to values in excess of 10^{5} S cm^{-1}. In order to understand the operation of polymer devices better, it is useful to first examine some basic properties of organic semiconductors based on conjugated polymers, because they differ qualitatively from those of crystalline inorganic semiconductors in several important respects.

In crystalline materials, the properties are determined by the three-dimensional arrangement of the atoms and their resulting interactions. Conjugated polymers are treated as a quasi-one-dimensional system, wherein the polymer chains

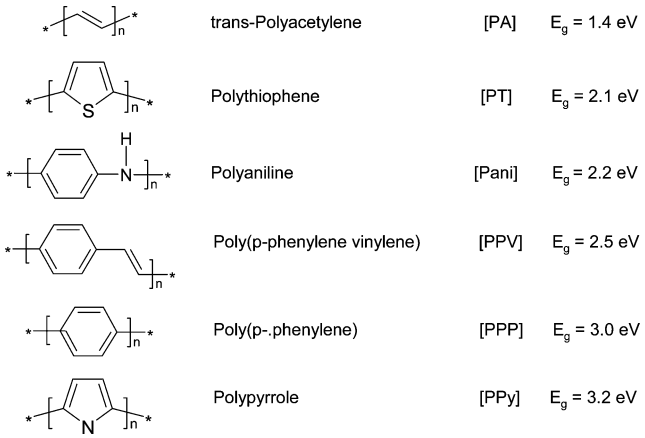

Figure 2. Schematic representation of the chemical structures of the most commonly studied conjugated polymers, as well as their corresponding nomenclature and energy band gap E_g.

are assumed to behave independently of one another, and their physical and chemical properties depend on interactions within the single chains. The π-bonding scheme of conjugated polymers decreases the gap between occupied (HOMO) and unoccupied (LUMO) states. The valence band and conduction band of conducting polymers are generally derived from such π-bonds. The band gap of these polymers tends to lie between 1.5 and 3 eV (see Figure 2), in the same range as that of inorganic semiconductors. Since the bonds formed by σ-orbitals are stronger than the π-bonds, the polymers do not break apart when excited states are created in the π-electron levels. Also, in most polymers, there is only a weak overlap between the π-orbitals between neighboring polymer chains, so electrons and holes tend to be delocalized on individual polymer chains, although they can hop between chains. The π-electron delocalization along the chain and the weak interchain bonding give conjugated polymers a quasi-one-dimensional nature and give rise to strong anisotropies when the macromolecules are chain extended and chain aligned. Due to the electron-phonon-coupling of the π-electrons, which leads to a lattice distortion (Peierls distortion), a gap is generated at the Fermi level. If an electron is added or removed to/from the polymer chain, a self-localized electronic state within the previously forbidden semiconductor band gap is formed as a result of the easy deformability of the polymer lattice without chain scissoring. The creation of electronic defects allows charge transport within a single chain. This property of conjugated polymers demonstrates that many ideas are used to explain why inorganic semiconductors do not directly carry over to conjugated polymers.

Early on, most of the research effort was concentrated on the conducting properties of the doped conjugated polymers,[32] which were often referred to as ''conducting polymers''. In this review, this notation is used throughout the text to describe this class of polymers when they are in both pristine and doped states.

2.2. Doping in Organic Semiconductors and Self-localized States

Doping of a disordered organic semiconductor by charged moieties has two counteracting effects: (1) the increase of concentrations of charge carriers and, thus, the change of the Fermi level;[33,34] (2) the increase of energetic disorder by formation of additional deep Coulomb traps of the opposite polarity. Therefore, the average hopping rate is controlled

by the charge carrier release from the Coulomb traps.[35] The former effect facilitates conductivity; the latter strongly suppresses the charge carrier hopping rate. This process determines, together with the intrinsic order, the temperature dependence of the mobility. Arkhipov et al. showed that the doping efficiency on charge carrier hopping strongly depends on the energy disorder and the external field.[35]

Upon doping by ionized species, charge neutrality must be maintained. There are two ways to accomplish this. One is electrochemical doping. If the ionization (or reduction) potential of the electrode more or less matches the HOMO of the organic semiconductor, a negatively charged majority carrier can be injected, provided that the electrolyte supplies appropriate counterions that can diffuse into the semiconductor. For p-conducting organic semiconductors, positively charged majority carriers are injected, as the oxidation potential of the electrode matches the LUMO. An example is the oxidation of polyhexylthiophene by injection of holes from a solution containing tetraethylammonium perchlorate. Charge injection is compensated for by concomitant "doping" with perchlorate anions. The alternative method is doping by a neutral entity, whose electron affinity is different enough to allow for charge transfer from the semiconductor to the dopant. In both cases, excess mobile majority carriers and immobile countercharges (i.e., dopants) are generated that roughen the energy landscape, in which the charge carriers migrate, but in the "neutral" doping case, in addition, charge redistribution can and does occur. The majority of charge carriers will actually form metastable geminate pairs, whose dissociation is facilitated by the ambient phonon bath and the external electric field.

A high charge carrier concentration can be reached without introducing counterions due to either field effect or high level of monopolar charge injection across a contact. Under these circumstances, the Coulomb interaction between charge carriers can strongly change the effective potential landscape. The interaction between charges of the same sign is repulsive and, therefore, cannot create Coulomb traps. It gives rise to transiently fluctuating potential barriers that affect the mobility.

2.2.1. Molecular Semiconductors

Doping of organic molecular films has been investigated relatively little compared to the doping of inorganic semiconductors or of conjugated polymers. The main reason is that, unlike inorganic semiconductors, traditional n- and p-doping has not been a requirement for achieving bipolar transport in the most common molecular devices, i.e., OLEDs and OFETs. The ability to stack electron and hole transport layers, to build organic/organic or metal/organic junctions, alleviates the need to "dope" the organic materials in order to inject electrons or holes into the active layer(s) of the organic device. However, the performance of organic devices is now reaching a level at which electrical doping seems to be attractive as a means to further improve efficiency. In this respect, considerable work remains to be done, however, to understand and control doping in materials which exhibit fundamental differences with standard inorganic semiconductors. The weak intermolecular bonds, large energy gaps, and small dielectric constants of these materials are not particularly conducive to low dopant ionization energies. Several groups have started to investigate doping mechanisms and their effect on the electronic structure of the host organic molecular semiconductors.[36−39] Particularly important are the relative energies of the dopant and the host molecular levels, which determine the ''ionization energy'' and doping efficiency. Doping of metal/organic contacts with inorganic donors, such as lithium in aluminum tris(8-hydroxychinoline) (Alq_3),[40] and with inorganic acceptors, such as antimony pentachloride in *N*,*N*′-diphenyl-*N*,*N*′-bis(3-methylphenyl)-1,1′-biphenyl-4,4′-diamine (TPD),[41] has shown the potential for significant improvements in current injection. Similar results could be obtained by doping with molecular acceptors, e.g., tetrafluorotetracyanoquinodimethane (F4-TCNQ),[37,42] and molecular donors, e.g., bis(ethylenedithio)tetrathiafulvalene (BEDT-TTF).[43]

2.2.2. Conducting Polymers

When an electron is added to (or withdrawn from) a rigid band semiconductor, it must go into the conduction band (or come from the valence band) because the lower energy valence band is completely filled. However, when an electron is added to (or withdrawn from) a conducting polymer, a chain deformation takes place around the charge, which costs elastic energy and puts the charge in a lower electronic energy state. The competition between elastic deformation energy and electronic energy determines the size of the lattice deformation, which can be on the order of 20 polymer units long.[44]

This localized charged particle together with the simultaneous chain deformation is known as a polaron and is defined in the semiconductor literature as an electron that is dressed by a phonon cloud. The lattice distortion by the charges is also called self-trapping. In Figure 3A, the doping process of p-type polypyrrole (PPy) is depicted, which represents a typical conducting polymer. The corresponding band structures and the allowed electronic transitions are shown in Figure 3B.

Bipolarons are similar to polarons, but they are double charged. Instead of being a single charge that distorts the chain, there are two charges, which are bound together in and by the same chain deformation. Although these charges repel each other via the Coulomb interaction, they remain bound together by their common chain deformation; the energy increase to form two distinct chain deformations rather than a single one is greater than the Coulomb energy gained by their separation.

Associated with each one of these excitations are energy states located in the energy gap of the p-doped polymer (Figure 3B). The polaron has two subgap states, of which the lower one is singly occupied and the higher one is empty for a positive polaron (i.e., an electron and a hole). The doubly charged bipolaron has its subgap states completely empty for a positive bipolaron. A significant difference between polarons and bipolarons is their spin signatures: polarons have charge ± 1 and spin $^1/_2$, the same spin and charge as a free electron. Bipolarons have a zero spin and are doubly charged, mainly because of the pairing of the electrons.

The charge injection into the macromolecular chain, i.e., the creation of any of the above-mentioned defects (polaron, bipolaron) in the conjugated backbone of the polymer, is called doping. Besides this charge injection, doping in polymers also implies the insertion or repulsion of a counterion (referred to as "dopants" or "doping ions") to maintain charge neutrality. In order to match conventions between physicists and chemists, a polymeric cation-rich material is called p-doped, and a polymeric anion-rich material is called n-doped. Since every monomer is a potential redox site, conducting polymers can be doped to a high density of charge carriers. The doping level is up to 5

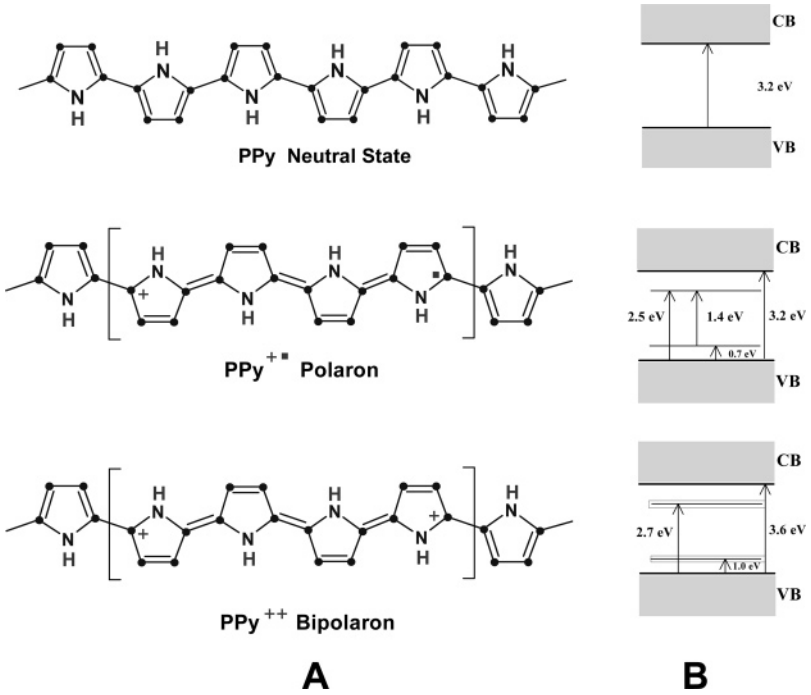

Figure 3. (A) Neutral (undoped) state of polypyrrole and doped (polaron and bipolaron) structures of lightly and heavily doped polypyrrole, respectively. (B) Corresponding schematic energy band structures and the allowed electronic transitions.

orders of magnitude greater than that in common inorganic semiconductors. The standard value of the doping levels lies in the range of 0.27−0.5 positive charge per monomer (27−50% by mol), depending on the anion and the type of conducting polymer. A slight decrease in the doping level is observed with an increase of the molecular weight and the negative charge of the anion. For all conjugated polymers, except for polyacetylene, polarons and bipolarons are the entities through which charge transport is accomplished in conducting polymers.[45] They can travel along the chain as an entity, with the atoms in the path changing their positions so that the deformation travels with the electron or hole.[46]

Doping in polymers can be accomplished chemically, electrochemically, and photochemically, as well as by charge injection at the metal/insulator/semiconductor (MIS) interface.[47] In the case of electrochemical and/or chemical doping, the induced electrical conductivity is permanent, until the charge carriers are purposely removed by dedoping, i.e., by reversing the electrochemical reactions, or until the charge carriers are chemically compensated.

Initially, conducting polymers have been regarded as one-dimensional semiconductors, because the π-conjugated systems extend over the whole polymer chains, thus allowing for delocalized states in one direction. In their pioneering work, Su, Schrieffer, and Heeger[48] studied the interaction of an excitation with an ideal one-dimensional lattice, neglecting Coulomb interactions and disorder effects. Today, conducting polymers are discussed either as one-dimensional semiconductors with strong electron/phonon interactions or as disordered molecular solids with strong Coulomb interactions. The discussion of the precise nature and dynamics of excited states in conducting polymers is still very much alive. The one-dimensional semiconductor nature of conducting polymers might play a role in experiments on highly ordered, stretch-oriented materials or on isolated single chains. Furthermore, in conducting polymers, the influence of chemical dopants on the morphology of the polymer layer and on the charge-transporting states is still a matter of controversy. The (quasi) one-dimensional nature of the conducting states may explain the exceptionally high conductivities in doped conducting polymer systems.[49]

2.3. Transport Mechanism in Organic Semiconductors

A feature common to all amorphous and disordered systems, among them organic semiconductors, is the frequency dependent conductivity that increases approximately linearly with frequency, at least in the range 10^1-10^7 Hz, i.e., $\sigma(\omega) \propto \sigma\omega^s$, where the frequency exponent $s \leq 1$.[50] The origin of this obviously universal behavior of the dispersive component σ_{ac} of the conductivity has been ascribed either to the relaxation process or to a transfer process. The former is caused by the motion of charge carriers by thermally assisted quantum mechanical tunneling between localized states lying deep within the band gap. The latter is called hopping and involves classical thermal activation over the barrier height, separating two sites with an energy difference ΔE. The frequency exponent s is predicted to have a temperature dependence, and the magnitude of s at any temperature is determined by the binding energy of the charge carrier in its localized site.[51]

The temperature dependence of the dc conductivity term provides first-hand information on the possible processes involved in the conduction in amorphous materials. One of the theoretical models most successfully used to predict the probable transport mechanism in disordered materials is the Mott's variable-range hopping (VRH).[52] It describes a phonon-assisted quantum mechanical transport process, in which a balance is obtained between the thermodynamics constraint on a charge carrier moving to a nearby localized state of different energy and the quantum mechanical constraint[53] on a charge carrier moving to a localized state of similar energy, but spatially far away. The VRH model is equally applicable to charge carriers such as electrons, polarons, or bipolarons, provided that the appropriate wave

function is incorporated. This model and its field of applications have been extensively reviewed by various authors.[52,54] According to the phonon-assisted quantum mechanical transport process, the temperature dependence of the dc conductivity provides information about the conduction mechanism and the dimensionality of the charge transport mechanism, which ranges from a three-dimensional to a one-dimensional transport process.

Considering a one-dimensional system, the most commonly invoked descriptions are charging-energy-limited tunneling (CELT),[55] fluctuation-induced tunneling (FIT),[53] and quasi-one-dimensional variable-range hopping.[52,56]

2.3.1. Molecular Semiconductors

Charge carrier hopping within a positionally random and energetically disordered system of localized states was shown to be an adequate model for the description of both the equilibrium and the nonequilibrium conductivity in noncrystalline organic semiconductors.[57−60] Bässler et al. discussed the effect of doping on the charge carrier hopping in disordered organic semiconductors.[58,61] Doping such a system by charged moieties will create a random distribution of dopant ions that will coulombically interact with charge carriers localized in randomly located intrinsic hopping sites[62] and, thus, broaden the effective density of states distribution. This effect is especially important for molecular semiconductors, because the dielectric permittivity is low, and the range of the Coulomb potential is large in organic solids.

2.3.2. Conducting Polymers

Much work has focused on the nature of charges in doped conducting polymers. Even though there is a high density of conduction electrons at the Fermi level for the highly doped polymers, the charge carriers may be spatially delocalized, so that they cannot participate in the electronic transport except through hopping. The prime source of localization in conducting polymers is structural disorder. Most conducting polymers are noncrystalline, i.e., amorphous materials, although some of these systems possess a molecular low crystallinity, in which regions of the material are more ordered and other regions are more disordered. The percentage of crystallinity may vary from near zero to 11% for polypyrroles,[63] 20−30% for polyanilines,[64] and approximately 80% for highly doped polyacetylenes.[65]

The charge carrier mobilities in these low-conducting amorphous solids are frequently estimated to be very low, $\mu \ll 1\ \mathrm{cm^2\ V^{-1}\ s^{-1}}$.[66] These values bear witness against a band transport mechanism. However, detailed knowledge of their charge transport is usually quite limited. Nevertheless, the basic principles underlying electronic states and electronic transport in this class of solid materials are those of amorphous solids. It should be emphasized that the great variety of polymer constituents and structures yields a diversity of interesting and perhaps specific electronic properties. The dimensionality of the system can play a major role in determining the nature of both electronic states and electronic transport. The intrinsic contributions to charge transport are strongly intermixed, and it is often not trivial to quantify the individual contributions from various parameters (e.g., interchain interactions, anisotropic diffusion of charge carriers, the role of dopant ions, the extent of disorder, etc.). The theoretical modeling of transport properties in conducting polymers is a challenging problem because of the extreme complexity of these systems.

For a transport mechanism to be described in a certain material, charge carriers must be present. In conducting polymers, upon injection of an electron or a hole, a defect in the polymer chain is created, i.e., a polaron or a bipolaron, as already mentioned. These charged defects are the real charge carriers in nondegenerated conducting polymers.

Charge transport in conducting polymers consists generally of two components: intrachain and interchain transport.[67,68] Intrachain charge transport occurs along the polymer backbone and requires less energy than interchain charge transport, which involves the hopping of the charge to neighboring chains. The dopant compounds play a very important role in the hopping process during interchain charge transport.

The charge carrier mobility may be thought of as a measure of the ease with which the charge carriers move through the material. It is sensitive to the level of structural order present in the polymer. Thus, structural defects decrease the conductivity by lowering the mobility. It is interesting that the theoretical conductivity of perfectly aligned defect-free polyacetylene is believed to be greater than $10^6\ \mathrm{S\ cm^{-1}}$.[67]

As a general consideration, the conjugation length appears to be the most significant structural parameter controlling the charge mobility. It has been recognized that the effective conjugation length of most conducting polymers is finite, because of the imperfect planarity of the conjugated system. It is supposed that the chain architecture of a conducting polymer consists of rigid blocks of a conjugation length of several polymer units separated by flexible nonconjugated polymer segments. This kind of macromolecular chain architecture should be kept in mind when one deals with the structure−property relationship of conducting polymers.

Currently, the description of the conductivity in these kinds of disordered materials remains open, and the understanding of the influence of the disorder, which is present at every scale of the structure (defects on the chains, heterogeneities in the doping distribution, etc.) is far from being complete. Moreover, several studies have been devoted to the theoretical search for microscopic pictures leading to different new descriptions, such as Fermi glass,[69] Coulomb glass,[70] superlocalization,[71] multifractal localization,[72] etc. Such a great variety of theoretical approaches reflects the wide range of phenomena involved in electronically conducting polymers. Furthermore, the transport process may differ from one polymer to another, as well as from one sample to another, principally according to the preparation method.

3. Metal/Semiconductor Junctions and Their Use in Gas Sensing

3.1. Introduction

In the following sections, the behavior of basic metal contacts with semiconducting materials and their application in chemical gas sensing are described. The elucidation of the interfacial electronic structure forms the basis for understanding and improving the performance of electronic devices. A key theoretical prediction is that the electric field at the semiconductor/metal interface should, in principle, respond to changes in the Fermi level of the contacting metal.[73,74] The behavior of such contacts has been discussed thoroughly in several books and reviews articles,[75−77] although the interfacial chemistry of these systems is still controversial.

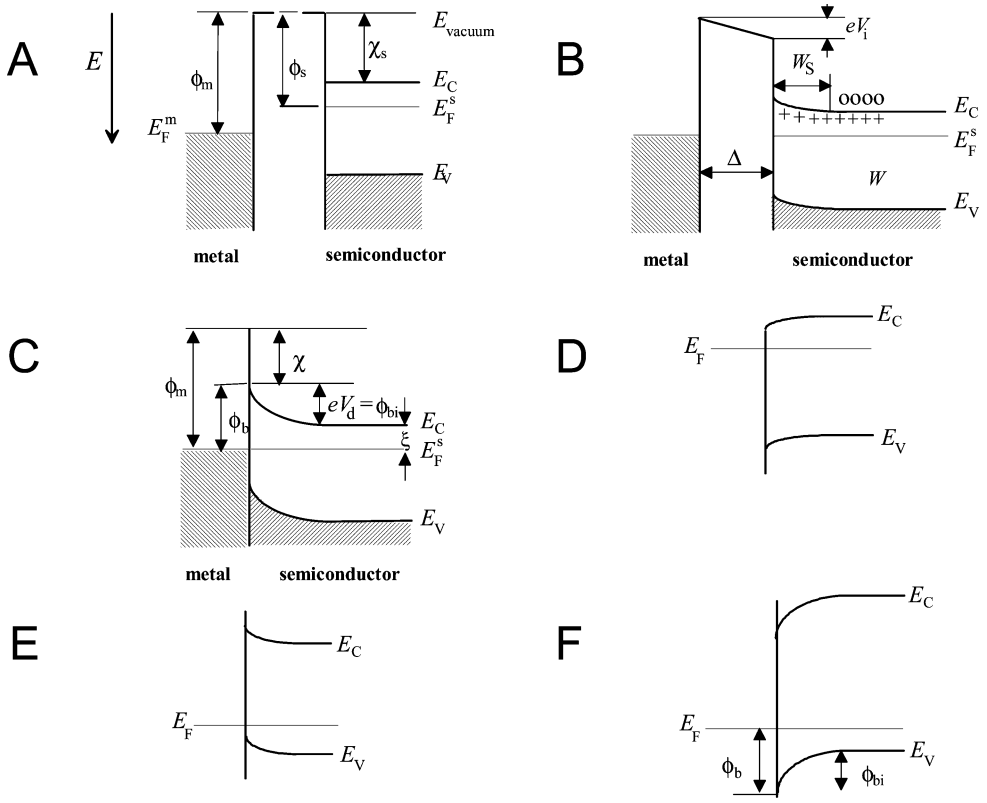

Figure 4. Formation of a barrier between a metal and a semiconductor: (A) neutral and isolated; (B) electrically connected; (C) in perfect n-type rectifying contact ($\phi_m > \phi_s$); (D) n-type ohmic contact ($\phi_m < \phi_s$); (E) p-type ohmic contact ($\phi_m > \phi_s$); (F) p-type rectifying contact ($\phi_m < \phi_s$). o denotes electron in conduction band; + denotes donor ion.

Metal/semiconductor contacts are components of any semiconductor device. At the same time, such contacts cannot be assumed to have a resistance as low as that of two connected metals. In particular, a large mismatch between the Fermi energy of the metal and the semiconductor can result in a high-resistance rectifying contact. A proper choice of materials can provide a low-resistance ohmic contact. However, for a lot of semiconductors, there is no appropriate metal available. Instead, one then creates a tunnel contact. Such a contact consists of a thin barrier, obtained by heavily doping the semiconductor, through which charge carriers can readily tunnel. Thin interfacial layers also affect the formation, which is discussed for metal/organic semiconductors contacts.

3.2. Interfacial Electronic Structure—Ideal Junction Characteristics

3.2.1. Formation of a Schottky Barrier

Experiments on rectifying contacts started in 1874 with the pioneering work of Braun, who observed asymmetries in the transport of electrical current across metal/semiconductor interfaces.[78] The following decades brought a variety of technical applications, but it took more than 60 years until Schottky,[79] and independently Mott,[80] used microscopic concepts to describe these so-called Schottky contacts. Since then, metal/inorganic semiconductor contacts have been extensively studied and have become rather well understood. The subject of interfacial electronic structure can be roughly divided into two aspects: (1) the energy level alignment at the interface and (2) the band bending in the space−charge region.[81] The former is important for charge carrier injection; the latter is essential for charge carrier separation. A complete overview of the works on Schottky contacts is beyond the scope of this review. Several excellent textbooks report on their electronic properties and the development of the field.[81−83]

Figure 4 illustrates the band diagram of Schottky's *Gedankenexperiment* for the formation of a Schottky barrier. The metal and the semiconductor are supposed to be electrically neutral and to be separated from each other for an n-type semiconductor with a work function ϕ_s smaller than that of the metal ϕ_m (Figure 4A). When the metal and the semiconductor come in electrical contact, the two Fermi levels are forced to coincide and electrons pass from the semiconductor into the metal. The result is an excess of negative charge on the metal surface and the formation of a positive charge depletion zone with a thickness W_S in the semiconductor near its surface (Figure 4B). These excess charges form an interface dipole and produce an electric field, directed from the semiconductor to the metal. By bringing the metal and the semiconductor closer together, the gap between the two materials vanishes and the electric field corresponds now to a gradient of the electron potential in the depletion layer, resulting in the well-known band-bending regime (Figure 4C).

The Mott−Schottky model leads to the Schottky barrier height ϕ_b. For an ideal contact between a metal and an n-type semiconductor, the height of the barrier ϕ_b measured relative to the Fermi level is given by

$$\phi_b = \phi_m - \chi_S \tag{1}$$

or

$$\phi_b = eV_d + \xi = \phi_{bi} + \xi \tag{2}$$

where χ_s is the electron affinity of the semiconductor, defined as the difference in energy between an electron at rest outside the surface and an electron at the bottom of the conduction band just inside the surface, e is the electronic charge, ξ is the difference between the bottom of the conduction band E_C and the Fermi level of the semiconductor, eV_d is the band bending at zero bias voltage, and eV_d, the diffusion potential at zero bias voltage, usually called the built-in potential ϕ_{bi} or the contact potential formed between the metal and the semiconductor, is given by[82]

$$\phi_{bi} = eV_d = \frac{eN_D W_S^2}{2\epsilon_S} \quad (3)$$

where N_D is the donor concentration, ϵ_s is the permittivity of the semiconductor, and W_S is the depletion layer width. Equation 2 has been referred to as the Mott−Schottky limit. In obtaining it, a number of important assumptions have to be made, namely that (1) the surface dipole contributions to ϕ_m and χ_S do not change when the metal and semiconductor are brought into contact, (2) there are no localized states on the surface of the semiconductor, and (3) there is a perfect contact between the semiconductor and the metal (i.e., there is no interfacial layer).

In the case that the work function of the n-type semiconductor ϕ_s is larger than that of the metal ϕ_m, the contact is biased so that electrons flow from the semiconductor to the metal. They encounter no barrier (Figure 4D). If a bias voltage is applied such that electrons flow in the reverse direction, the comparatively high concentration of electrons in the region where the semiconductor bands are bent downward (usually referred to as the accumulation region) behaves like a cathode, which is easily capable of providing a copious supply of electrons. The current is then determined by the bulk resistance of the semiconductor and the applied voltage. Such a contact is termed ohmic contact.

A p-type semiconductor/metal junction, for which ϕ_m exceeds ϕ_S, represents an ohmic contact (Figure 4E). The case of a p-type semiconductor, for which ϕ_S exceeds ϕ_m, is shown in Figure 4F. Bearing in mind that holes have difficulty in going underneath a barrier, one sees that Figure 4F is the p-type analogue of Figure 4C and gives rise to rectification, which is the case of Schottky contacts based on p-type organic semiconductors. The barrier height ϕ_b for an ideal contact between a metal and a p-type semiconductor is given by

$$\phi_b = E_g - (\phi_m - \chi_s) \quad (4)$$

3.2.2. Charge Carrier Transport Mechanism across the Junction Potential Barrier

The models initially developed for charge carrier transport across potential barriers in crystalline materials have also been used for noncrystalline systems. The current across a metal/semiconductor junction is mainly due to majority carriers. Three distinctly different mechanisms exist: diffusion of charge carriers from the semiconductor into the metal, thermionic emission of charge carriers across the Schottky barrier, and quantum mechanical tunneling through the barrier. The diffusion theory assumes that the driving force is distributed over the length of the depletion layer. The thermionic emission theory, on the other hand, postulates that only energetic charge carriers, which have an energy equal to or larger than the conduction band energy at the metal/semiconductor interface, contribute to the current flow. Quantum mechanical tunneling through the barrier takes into account the wave-nature of the electrons, allowing them to penetrate through thin barriers. In a given junction, combinations of all three mechanisms exist. However, typically one finds that only one charge carrier mechanism dominates.

Thermionic Emission Theory. Thermionic emission theory assumes that the barrier height ϕ_b is much larger than kT and that electrons, with an energy larger than the top of the barrier, will cross the barrier, provided they move toward the barrier. The actual shape of the barrier is hereby ignored. The current density, J, can be expressed as

$$J = A^{**}T^2 \exp\left(\frac{\phi_b}{kT}\right)\left[\exp\left(\frac{eV}{kT}\right) - 1\right] \quad (5)$$

or

$$J = J_0\left[\exp\left(\frac{eV}{kT}\right) - 1\right] \quad (6)$$

where A^{**} is the effective Richardson constant for thermionic emission, neglecting the effects of optical phonon scattering and quantum mechanical reflection (equal to 120 A cm^{-2} K^{-2} for free electrons), T is the absolute temperature, k is the Boltzmann constant, V is the bias voltage, and J_0 is the saturation current density, given as

$$J_0 = A^{**}T^2 \exp\left(-\frac{\phi_b}{kT}\right) \quad (7)$$

Diffusion Theory. For semiconductors with low charge carrier mobility ($\mu < 10^{-4}$ cm^2 V^{-1} s^{-1}), it has been shown that the dominant barrier transport mechanism is diffusion.[81] The diffusion theory by Schottky[81] is derived from the assumption that the depletion layer is large compared to the mean free path, so that the concepts of drift and diffusion are valid. The resulting current density equals

$$J = eN_c\mu_e\ddot{E}_{max} \exp\left(-\frac{\phi_b}{kT}\right)\left[\exp\left(\frac{eV}{kT}\right) - 1\right] \quad (8)$$

or

$$J = J_{SD}\left[\exp\frac{eV}{kT} - 1\right] \quad (9)$$

where N_C is the effective density of states in the conduction band, μ_e is the electron mobility, and $\ddot{E}_{max}$ is the maximum field strength at the metal/semiconductor interface given by $\ddot{E}_{max} = eN_D W/\epsilon_s$. It can be seen that eq 9 is almost, but not quite, of the form of the ideal rectifier characteristic for thermionic emission. The difference arises because $\ddot{E}_{max}$ is not independent of bias voltage but is proportional to $(V_0 - V)^{1/2}$. For large values of reverse bias, the current does not saturate but increases roughly with $|V|^{1/2}$.

3.2.3. Ohmic Contact and Space Charge Limited Current

A metal/semiconductor junction results in an ohmic contact (i.e., a contact with voltage independent resistance), if the Schottky barrier height ϕ_b is zero or negative. In such cases, the charge carriers are free to flow in and out of the semiconductor so that there is a minimal resistance across the contact (see Figure 4D and E). For an n-type semiconductor, the work function of the metal must be close to or smaller

than the electron affinity of the semiconductor. For a p-type semiconductor, it requires that the work function of the metal must be close to or larger than the sum of the electron affinity and the band gap energy. Since the work function of most metals is less than 5 V and a typical electron affinity is about 4 V, it can be problematic to find a metal that provides an ohmic contact to p-type semiconductors with a large band gap such as GaN, SiC, or organic semiconductors. The values of the work function of organic semiconductors strongly depends on the preparation method and the doping level. The values range between 4.0 and 5.3 and can even differ for the same type of polymer and doping because of differences in the treatment of the material. Therefore, the reader is referred to the literature to obtain information on the work function values of the organic semiconductors of interest.

Effect of Background Doping−Bulk Limited Transport. In $J-V$ characteristics, a slope of the ln J versus ln V plot of approximately unity indicates an ohmic conduction. Assuming conduction is via holes, the current flow may be expressed in the form[84]

$$J = eh_0\mu_h\left(\frac{V}{L}\right) \tag{10}$$

where h_0 is the concentration of thermally generated holes in the valence band, μ_h is the hole mobility, and L is the thickness of the semiconductor. The concentration of holes at thermal equilibrium is given by

$$h_0 = N_V \exp\left[-\frac{(E_F - E_V)}{kT}\right] \tag{11}$$

where N_V is the effective density of states in the valence band and $(E_F - E_V)$ is the separation of the Fermi level from the valence band edge. The current density in the ohmic region becomes

$$J = e\mu_h N_V\left(\frac{V}{L}\right)\exp\left[-\frac{(E_F - E_V)}{kT}\right] \tag{12}$$

By plotting ln(J/V) against 1000/T, the values $e\mu_h N_V$ and $(E_F - E_V)$ can be calculated from the slope and the intercept at $1/T = 0$.

When holes are injected into the p-type bulk of a metal/p-type semiconductor Schottky diode, the total hole density $N_V(x)$ at the point x measured from the ohmic (metal) contact consists of two parts: (1) the density of the existing holes h_0 induced by the background acceptors and (2) the density $[N_V(x) - h_0]$ of the injected holes. The total density of the holes determines the current. The space charge is determined by the distribution of injected holes, provided that the charge of the existing holes h_0 is compensated by the ionized fixed dopant ions. As long as the total hole density $N_V(x)$ is equal to the doping density over most of the sample thickness, there is no space charge present, and it is expected that Ohm's law will be obeyed. The electric field in the doped samples becomes constant over practically the whole length of the sample. This assumption would be equivalent to performing an electrochemical experiment in which the resistance of the solution dominates and no electrochemical activity at the surface electrode (i.e., contact) can be detected. In effect, such a case corresponds to a chemiresistor in which the useful information is obtained from the changes of bulk resistivity of the sensing layer. This is not the case for Schottky barrier junctions.

If current is passing through a forward biased junction with a low doped semiconductor or a semiconductor exhibiting low mobility, a depletion layer will be formed in front of the ohmic contact of the Schottky barrier diode, as discussed by Chen et al.[85] It can be described in analogy to the depletion polarization effect in an electrochemical experiment by a limited charge carrier transport process inside the semiconductor toward the ohmic contact. The width of the mass-transport limited contact resistance can be modulated by the external field. The time dependence of the polarization resistance is controlled by the charge carrier mobility and by the geometry of the contact. In most Schottky barrier devices, the ohmic contact resembles an electrode with a rectangular geometry, for which the polarization resistance increases with $1/\sqrt{t}$ at constant applied voltage. The current increases roughly with $|V|^{1/2}$ (see also section 3.2.2).

Moreover, a second bulk effect has to be taken into account in the presence of an intrinsic or low doped semiconductor forming the Schottky barrier junction. If the semiconductor has no free or low charge carrier density due to doping or due to intrinsic thermal ionization, the theory of space charge limited current (SCLC) applies and the current density J is given by the V^2 (Mott−Guerney) Law[81,86]

$$J = \frac{9}{8}\epsilon_s\mu\frac{V^2}{L^3} \tag{13}$$

where ϵ_s is the permittivity of the semiconductor and L is the thickness of the sample. With increasing applied voltage, the charge carrier density of the undoped sample increases continuously with x. The injected charge carrier density becomes considerably larger than the doping induced density in most of the volume of the sample and the electric field increases with $\sqrt{x}$.

The behavior of the current density at high currents, and therefore at high voltages, is quite different. The curves for high and low doped semiconductors become identical. One would therefore expect that the current would obey the SCLC V^2 law at high voltages in the doped material as well.

The transition from Ohm's law to SCLC takes place at the point at which the Ohm's law straight line and the SCLC line (corresponding to the V^2 law) meet. Therefore, an expression for the voltage V_{tr}, at which the transition occurs, can be derived by equating the ohmic current and the SCLC (eqs 10 and 13):

$$V_{tr} = \frac{8eh_0L^2}{9\epsilon_s} \tag{14}$$

This equation provides a method for determining the background doping concentration. The transition voltage V_{tr} can be experimentally determined.

Effect of Trapping and Field Dependent Mobility. A modification of the V^2 law occurs when trapping and the dependence of the mobility on the electric field are taken into account. The effects of trapping and field dependent mobility on the $J-V$ curves have been discussed by several authors.[86−89] Most workers have assumed an exponential distribution of traps N_{tr} given by

$$N_{tr}(E) = N_V \exp\left(-\frac{E}{kT_{tr}}\right) \tag{15}$$

where N_V is the density of states for a p-type semiconductor

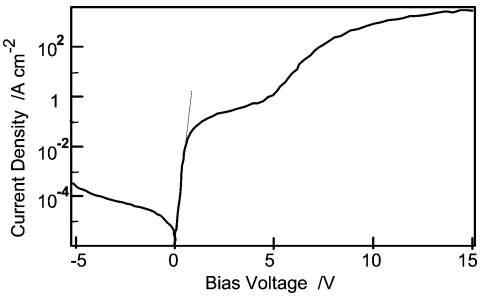

Figure 5. Dark $J-V$ characteristic of an Al/doped PPy Schottky diode. The dashed line indicates the fit of ln J vs V according to thermionic emission (see section 3.2.2).

and T_{tr} is the characteristic temperature of the distribution. The ratio of free to trapped charge carrier density θ for a p-type semiconductor is given by

$$\theta = \frac{N_V}{N_{tr}} \exp\left[\frac{-(E_t - E_V)}{kT}\right] \tag{16}$$

where $(E_t - E_V)$ is the activation energy of hole traps. For the distribution of traps, the current density J is given by the $J = k_{tr}V^m$ power law, where k_{tr} is a constant and the value of the exponent m depends on the characteristic temperature T_{tr}. The effect of field dependent mobility has also been discussed by several authors.[89,90] Most authors have used the following equation for the mobility:

$$\mu = \mu_0 \exp(\beta\sqrt{E}) \tag{17}$$

Variations of this equation are discussed by Campbell et al.[89] It is shown that both SCLC with traps and field dependent mobility can give rise to the equation $J = k_{tr}V^m$. However, experimental currents measured at different temperatures could not be described with one value of m. At a given temperature and in a small voltage range, the V^m law with constant m has been experimentally verified.[89]

Figure 5 shows a typical current density vs applied voltage curve of an Al/PPy Schottky diode. The diode is forward biased at positive voltages, implying that the Al contact is negative. The current density in the low bias region between 0.1 and 1.5 V varies exponentially with the bias voltage and fits closely with the thermionic emission theory (eq 6). At a bias voltage > 1.5 V, the current starts to become linear, indicating a dominant contribution of the bulk resistance, which is in series with the resistance of the depletion layer of the diode. As the voltage increases to more than 5 V, the current increases again. This indicates the transition from the contribution of the ohmic current to the contribution of the SCLC, according to eq 14. The current density J varies with V^m. The determination of the exponent m by plotting J as a function of V^m gives information if the SCLC regime is trap free and the mobility is field independent ($m = 2$) or controlled by trapping or by the effect of the electric field on the mobility ($m > 2$).

3.2.4. Tunneling through the Barrier

An alternate and more practical contact is a tunnel contact, if no appropriate metal is available to form an ohmic contact. It can be particularly problematic to find a metal that provides an ohmic contact to doped organic semiconductors that usually show work functions of about 5 V or higher. Tunnel contacts do have a positive barrier at the metal/semiconductor interface. They also have a high enough doping level in the semiconductor that there is only a thin barrier separating the metal from the semiconductor. For heavily doped semiconductors (doping level: 10^{19} cm^{-3} or higher) exhibiting a depletion region width at the metal/semiconductor interface on the order of 3 nm or less, or for operation at low temperature, it may be possible for electrons with energies below the top of the barrier to readily tunnel across such barriers by quantum mechanical tunneling.[82] If the tunneling current dominates the current flow, the current−voltage relationship is of the form

$$J = J_0 \exp\left(-\frac{\phi_b}{E_{00}}\right)\left[\exp\left(\frac{eV}{kT}\right) - 1\right] \tag{18}$$

where $E_{00} = (h/4\pi)(N_D/m^*\epsilon_s)^{1/2}$/eV, where h is Planck's constant and m^* is the effective mass of the electron. The equation indicates that the tunneling will increase exponentially with $\sqrt{N_D}$.

A possible mechanism for the charge transfer from the metal to a conductive polymer based on tunneling through the barrier is given by Gustafsson et al.[91] Mobile charges in the conducting polymer exist in the form of polarons and bipolarons which occupy states in the band gap (see section 2.2.2). They are different from the valence band holes normally encountered in inorganic semiconductors. Injection of a hole by tunneling or by thermionic emission into the polymer should be similar to the photogeneration of charge in conducting polymers, where, after its formation, a rapid relaxation to polaronic/bipolaron states occurs.[92] Thus, the majority carrier transfer from the metal to the polymer is based on (1) tunneling through the barrier to the valence band, followed by (2) an immediate relaxation to a polaron or bipolaron defect state, whereas, in the opposite direction, the charge transfer occurs by direct tunneling from the defect state to the metal. This gives rise to different tunneling paths at different energy levels in the forward and reverse bias voltage directions, which probably can affect the rectification ratio of the device.

3.3. Interfacial Electronic Structure—Deviations from the Ideal Case

3.3.1. Introduction of the Ideality Factor

Real Schottky diodes do not always follow the expressions derived for the ideal case of a charge carrier transport mechanism across a potential barrier. Deviations from ideal behavior arise from imperfections in fabrication, or factors, which are not included in the relatively simple theories taken for derivation of eqs 5−9 and eq 18. A few of the major limitations are given below. In practice, diodes never satisfy eq 5 exactly but can be more closely described by the modified eq 19.[82]

$$J = J_0 \exp\left(\frac{eV}{nkT}\right)\left[1 - \exp\frac{eV}{kT}\right] \tag{19}$$

or

$$J = J_0 \exp\left(\frac{eV}{nkT}\right) \quad \text{for} \quad V \gg \frac{3kT}{e} \tag{20}$$

where n is the ideality factor, which can be estimated from the slope of the straight part of the ln J vs V plot and is usually greater than unity. The ideality factor n is introduced in eq 19 to account for the failure of the simple, single-

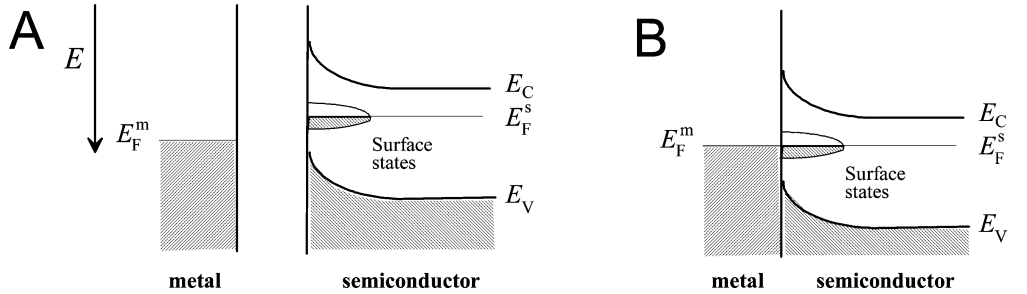

Figure 6. Schematic band diagram of the band bending interface in the presence of surface states for a metal/semiconductor: (A) before contact; (B) after contact formation. The Fermi level is pinned by a high density of surface states of the semiconductor.

carrier theories of barrier behavior, e.g., when image lowering of the potential barrier occurs. There are many other possible reasons why n should exceed unity, e.g., series resistance of the bulk semiconductor, generation-recombination within the depletion region, tunneling through the barrier, interface states, and the presence of an insulating interfacial layer.[82,93] In the case of polymeric diodes, bulk resistance and interfacial layer effects are likely to be the most important.

3.3.2. Schottky Barrier Lowering

It has been assumed that the Schottky barrier height remains constant under all conditions of applied voltage. However, the barrier height varies with applied voltage because conduction electrons experience a force from their image charges in the metal. This force attracts the electrons toward the metal surface, effectively lowering the barrier and allowing voltage-dependent deviations from ideal behavior. In theory, this "image force" should give the reverse current a fourth-power dependence of bias upon voltage, rather than the constant value implied by eq 7. This effect is usually not observed, because charge carrier generation in the depletion region at high reverse bias and tunneling effects dominate the reverse leakage. At forward biases above approximately 0.1 V, the effect causes a slight deviation of the ideality factor n from unity. For a diode that is assumed to be ideal except for barrier lowering, the ideality factor is

$$n = \left(1 - \frac{\mathrm{d}\phi_b}{\mathrm{d}V}\right)^{-1} \tag{21}$$

where $\mathrm{d}\phi_b/\mathrm{d}V$ is the derivative of the barrier height with respect to the applied voltage. The image force lowering of the barrier $\Delta\phi_{bi}$ is given as

$$\Delta\phi_{bi} = \left(\frac{e\ddot{E}_{max}}{4\pi\epsilon_0}\right)^{1/2} \tag{22}$$

$\ddot{E}_{max}$ is the maximum field at the interface, and $\epsilon_0 = 8.85 \times 10^{-14}$ C cm^{-1} V^{-1} is the permittivity of free space.

3.3.3. Effect of Interface States

Very often, a deviation from the ideal Mott−Schottky behavior is observed. It can be measured in terms of the slope parameter

$$S = \frac{\mathrm{d}\phi_b}{\mathrm{d}\phi_m} \tag{23}$$

describing the dependence of the Schottky barrier height on the metal work function. According to the Mott−Schottky model, S should be equal to unity, while S is smaller than unity for any deviation.

An important limitation of the Mott−Schottky model is the neglect of intrinsic surface states with energy levels located in the semiconductor band gap which are pinning the metal Fermi level as shown in Figure 6. In this extreme case, the Schottky barrier height does not depend at all on the metal work function, i.e., $S = 0$.

Considering a continuum of interface states, a phenomenological formula for the Schottky barrier height can be formulated[76]

$$\phi_b = S(\phi_m - \chi_s) + (1 - S)\phi_0 \tag{24}$$

where S is the slope factor and ϕ_0 is the barrier height when the charge neutrality level of the continuum of interface states coincides with the Fermi level at the interface. The barrier height becomes independent of the metal work function and is determined entirely by the doping and surface properties of the semiconductor. In real situations, the constant S lies between 0 and 1. "Fermi level pinning" indicates that the Fermi level position at the surface of the semiconductor measured relative to the vacuum level does not vary when either the work function or the Fermi level or the contacting phase is varied. Under strong Fermi level pinning, a constant electric potential is dropped across the semiconductor regardless of the nature of the metal. The remaining potential is dropped across a thin dielectric layer near the metal/semiconductor junction.

Besides the interface states, other reasons have been proposed for inorganic semiconductor/metal junctions as explanations for the Fermi level pinning behavior, i.e., chemical reactions such as alloy formation,[94] or other stoichiometry changes,[95] and/or quantum mechanically induced interface states.[96] Although these theories were primarily developed to explain the behavior of inorganic semiconductor/metal contacts, many of them also make testable predictions regarding the behavior of contacts comprising organic semiconductors in Schottky barrier junction sensors.

3.3.4. Metal/Organic Semiconductor Junctions with an Interfacial Layer

The elucidation of the interfacial electronic structure, particularly the energy-level alignment at organic/substrate interfaces, forms the basis for understanding and improving the performance of organic electronic devices.[97,98] Despite the advances in device application, there is still only a limited understanding of the interface between organic materials and metals. A number of recent studies have helped to understand the basic properties of the interface; see, e.g., the review by

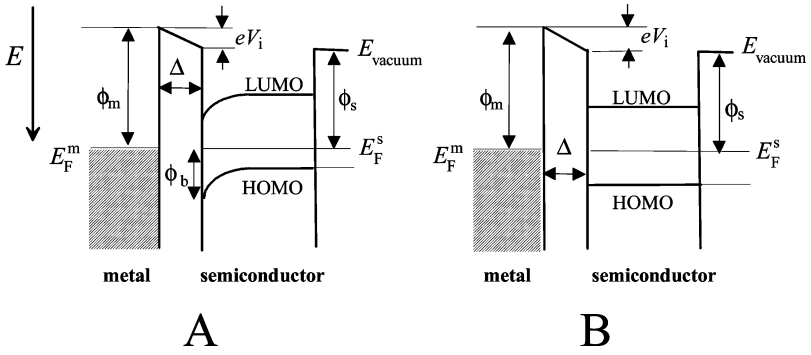

Figure 7. Energy diagram of the organic/metal interface with (A) band bending leading to Fermi level alignment and (B) without band bending. E_{vacuum} denotes the vacuum level, E_F is the Fermi level, eV_i is the shift of the vacuum level at the interface due to the dipole layer formation, and Δ is the interfacial layer thickness.

Seki at al.[99] and references therein. In particular, ultraviolet and X-ray photoemission spectroscopy (UPS, XPS) have been used to investigate metal/organic[100,101] and organic/organic[102−104] interfaces. The organic layers employed in such studies were nominally undoped, although the purity of the organic layers is usually insufficient to achieve intrinsic behavior.

The simplest model used to discuss the energy level offset at these interfaces is the "vacuum-level alignment" model (i.e., Mott−Schottky limit, eq 2). The band of an organic semiconductor in contact with a metal is bent to achieve the alignment of the Fermi level of the metal with the Fermi level of the organic layer fixed somewhere in the band gap, simply by analogy to an interface between a doped inorganic semiconductor and a metal.

As shown for several interfaces between an undoped organic semiconductor and a metal layer prepared in UHV, this is not always true.[105] If the Fermi level fixing and its alignment with the metal Fermi level occur by atmospheric doping for an organic semiconductor, this assumption may become valid for practical devices prepared and used under atmospheric conditions such as ambient air. The doping process is expected to cause a characteristic band bending at organic semiconductor/metal interfaces. Several problems have remained in understanding whether or not this simple model is applicable to typical organic/inorganic and organic/organic interfaces. Among these, the two main problems are (1) little is confirmed experimentally about the effects of the molecular orientation and/or packing structure on electronic structures near organic/organic and organic/inorganic interfaces and (2) it is not easy to clearly distinguish the electronic structure in the "contact interface" from that in the bulk region.[106] Changes in the molecular orientation during film growth may cause unintentional dipole-layer formation in the film[107] and unintentional changes in the ionization potential of the film.[108] In contrast, several groups have reported the electronic structure of a well-defined organic/substrate contact interface.[109−111]

The organic/substrate interface can be divided into two adsorption systems:[99] (1) a chemisorbed system, in which the interface dipole is formed by chemical interactions and electron transfer, which gives rise to pinning of the energy levels of the organic semiconductor to the substrate Fermi level, independent of the initial semiconductor work function, and (2) a physisorbed system, in which the interface dipole is formed by the push-back effect and electron transfer.

The important aspects can be discussed using Figure 7. When a metal and an organic solid come into contact, a dipole layer may be formed right at the interface, due to rearrangement of electronic charge. Several mechanisms have been identified to explain this type of interface dipole.[38,112] Possible origins of the rearrangements are, e.g., charge transfer across the interface, redistribution of the electron cloud spilled out of the metal surface, mirror force, formation of an interfacial electronic state, interfacial chemical reaction, and aligned permanent dipoles of adsorbed molecules.[99] Such interfacial dipole layer formation results in an abrupt shift of the potential across the dipole layer, leading to a shift of hypothetical vacuum levels (eV_i) at the interface, as shown in Figure 7.

If the organic semiconductor is doped, for example by an acceptor, as shown in Figure 7A, the dopant can be ionized to form a fixed space charge, and the energies of the occupied and unoccupied levels are shifted with increasing distance from the interface, indicating the space−charge region at the metal/semiconductor interface. However, most organic semiconductors are used, at least nominally, undoped and the electronic structure of the semiconductor is represented without surface "band bending", as shown in Figure 7B.

The presence of a space−charge region at the interface between a doped semiconductor and a metal, with a significant molecular level bending in the doped layer, has been amply demonstrated.[39,113] The magnitude of the space−charge region has also been shown to be larger in wide band gap semiconductors with low intrinsic charge carrier concentrations and low conductivity,[114] which are common characteristics of organic semiconducting materials.

Nishi et al. discussed the effect of bulk oxygen doping on the interfacial electronic structure of titanyl phthalocyanine films (TiOPc) deposited on various metal substrates.[105] Films prepared under UHV did not show the alignment of the metal Fermi level with the Fermi level of the organic semiconductor at fixed energy within the band gap, as shown in Figure 7B, possibly because of insufficient charge density in the TiOPc films. On the other hand, there is a conversion from n- to p-type semiconductor seen, when the film is exposed to O_2, as well as a clear alignment of the Fermi level together with the formation of a space−charge region and an upward molecular level bending (Figure 7A).

Heeger et al. presented a model to understand the interactions at doped polymer/metal interface[48,115] which was refined by Brazovskii et al.[116] The model considers specifically the charge carriers in degenerated conjugated polymers. The nondegenerate continuum model of Davids et al.[117] extended the work toward conjugated polymers with a nondegenerate ground state. Based on the relative energies between the Fermi level of the metal (E_F) and the formation energy of polarons and bipolarons of the polymer, E_{form},

conclusions about the extent of charge transfer during interface formation can be made. If E_F of the contact is higher in energy than the E_{form} of the negative bipolaron/polaron, the transfer of a large negative charge density into the polymer occurs, whereas a large positive charge density is transferred if E_F of the contact is lower than E_{form} of the positive bipolaron/polaron. In addition, Davids et al. suggested that the presence of traps in the polymer will accommodate charges as well.[117] After values are assigned to the polaron and bipolaron formation energies, as well as to the trap energies and densities, it is possible to model the potential and charge density at the metal/polymer interface for a given Fermi energy with respect to the center of the energy gap by solving the Poisson equation. As a result, the transferred charge remains close to the metal/polymer interface.

By considering the metal/polymer interactions from the microscopic point of view of quantum interactions, a molecular modeling was carried out, which took into account the quasi-one-dimensionality of the polymer system.[118−120] As a result of the difference in the Fermi levels of the metal and the conducting polymer, it is expected that charge transfer may occur across the interface. Furthermore, the quantum calculation approach considers specific chemical reactions or even charge donation between the metal and the polymer as a result of bringing metal atoms in the vicinity of a conjugated system and observing the changes in the electronic structure of the resulting system. Based on such calculations, it has been postulated that the metal plays an important role in determining the extent of charge transfer that occurs in metal/conducting polymer interfaces: Ca and Na appear to transfer charge at the interface without significantly altering its chemistry.[118,119] Al, on the other hand, disrupts the chemical structure of the surface of the conducting polymer.[119] The results obtained in the case of Ca and Na agree with the general behavior postulated by Davids et al.,[117] whereas Al deposition introduces an additional effect of surface chemical reactions, which are not considered by the continuum model.

3.4. Gas/Solid Interactions in Schottky Barrier Junction Devices

The key difference between organic and inorganic Schottky barrier junction devices is the ability of many gases and vapors to penetrate through the organic semiconductor either to change the Schottky junction resistance or to interact with the semiconductor itself, which causes a work function change of the material, as shown in section 3.4.1. In the case of an inorganic Schottky barrier junction device, gas permeation toward the metal/semiconductor interface works only for hydrogen or hydrogen-producing compounds and then gives rise to formation of a dipole layer, as discussed in section 3.4.2. Adsorption at the catalytic metal surface has only a limited secondary effect, i.e., the dissociation of molecular hydrogen to atomic hydrogen.

3.4.1. Bulk Effect upon Gas Doping—Modulation of the Electron Work Function

The rectifying behavior of the Schottky diodes relates directly to the Fermi level of the layer of the organic semiconductor and can be influenced not only by the structure, the dopant type, and the doping level,[121] but also by the interaction of the semiconductor with gases or vapors. By exposure of the organic semiconductors to certain gaseous species exhibiting electron donor or acceptor behavior, the Fermi level position is changed[27,30,122] by either a decrease or an increase in the doping level. In this case, a gas-induced change of the Schottky barrier characteristics can be observed, which can be exploited for gas sensing measurements.

In 1980, Van Ewyk et al. proposed the formation of a charge-transfer complex due to an electron donator/acceptor interaction during the absorption of strong electron donating or accepting gases on organic p-type semiconductors.[123] The absorption causes a change in the doping level of the semiconductor and thus a change in its conductivity. The transfer of a partial amount of electron density without complete ionization of the reacting species is generally known for adsorption processes of molecules on conducting surfaces and has been treated comprehensively, from both the catalysis[124] and chemical[125] points of view. It was assumed that this type of reaction is also responsible for the chemical modulation of the electron work function of the polymer layer due to gas absorption.[126]

This type of interaction process is often described as a secondary doping of the sensitive semiconducting layer. The primary doping process is carried out during formation of the semiconducting sensing layer by incorporating doping ions. In the case of an organic semiconductor, primary doping is carried out during the chemical or electrochemical preparation process.[67,127]

Janata presented a model that describes the potential concentration relationship based on the formation of a charge-transfer complex between the secondary dopant (gas or vapor) and the matrix (sensitive phase), which is combined with a fractional charge transfer δ.[128]

The dependence of the Fermi level position of the sensitive material on the partial pressure, p_{gas}, of the dopant gas or vapor is given by

$$E_F = E_0^* + \frac{kT}{2\delta}\ln(p_{gas} + \text{const}) \quad (25)$$

where in E_0^* the donor/acceptor level of the organic semiconductor and the equilibrium coefficients of all relevant reactions are combined. For $p_{gas} = 1$, E_F equals E_0^*, denoted as the value of the Fermi level under standard conditions. A change of the Fermi level is reflected in the change of the work function E_{WF} of the semiconductor

$$\Delta E_F = \Delta E_{WF} \quad (26)$$

Equation 25 has the familiar form of the Nernst equation for ion and electron transfer across the interface of two condensed phases, except that they account for the fractional charge transfer δ. The magnitude and the polarity of the response depend on the value of the charge-transfer coefficient δ, and with $2|\delta| < 1$, a fractional value of the slope is possible. It depends on the ability of the entering gas or vapor molecules to exchange charge density with the semiconductor matrix either by oxidizing ($2\delta < 0$) or reducing ($2\delta > 0$) the active sites of the matrix. The gas/vapor behaves like an electron acceptor and donor, respectively.

In the absence of interfacial layer and Fermi level pinning, the gas-induced change of the Fermi level causes a change in the Schottky barrier characteristics in the low bias region. The diode current is then exponentially related to the change of the Fermi level, i.e., the work function of the semiconductor and the applied voltage, according to eq 5.

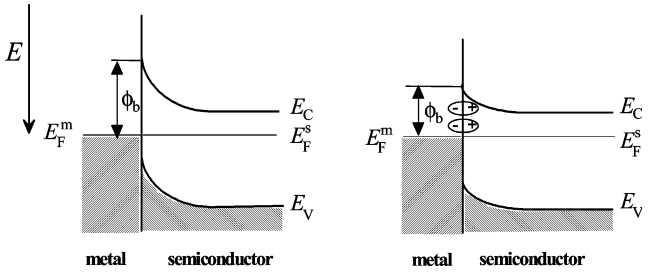

Figure 8. Band diagrams of a catalytic metal/semiconductor Schottky diode without and with hydrogen adsorption, respectively.

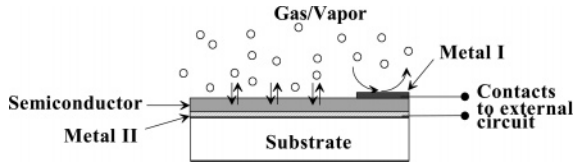

Figure 9. Cross-sectional view of a typical geometrical arrangement of a Schottky barrier diode used for chemical sensing applications.

3.4.2. Formation of a Dipole and an Interfacial Layer

It is known that a number of metals, e.g., palladium or platinum, adsorb and dissolve hydrogen and that the adsorbed atoms change the work function of the metal surfaces. By using a thin metal film as the catalytic metal electrode of the Schottky diode, hydrogen and other gases that react with the catalytic metal can be detected.

Hydrogen molecules are adsorbed and dissociated on the outer metal surface. Then, the atomic hydrogen permeates through the bulk lattice toward the metal/semiconductor, causing a perturbation at this interface that gives rise to a change in the sensor output signal. Two hypothetical steps were proposed to explain the detection mechanism:[129] (1) the hydrogen atom is polarized at the metal/semiconductor interface, which gives rise to a dipole layer, or (2) an excess of charge states at the metal/semiconductor interface is created in the presence of hydrogen and reduces the Schottky barrier height.

Figure 8 illustrates the band diagrams without and with hydrogen adsorption, respectively. The hydrogen-polarized layer, arising from the intrinsic electric field of the diode, redistributes the charges in the depletion region and abates the degree of band bending. Hence, the corresponding current is correlated with the number of hydrogen atoms adsorbed at the metal/semiconductor interface.

When atomic hydrogen has been formed on the outer metal surface, which is exposed to the ambient (see Figure 9), an equilibrium between the hydrogen concentration at this metal surface and that at the metal/semiconductor interface is reached. Based on this model, the change in the $J-V$ characteristics and the decrease in the Schottky barrier height are strongly related to the hydrogen concentration. Assuming that the adsorption is not affected by conditions outside the metal surface, the metal/semiconductor interface has similar adsorption properties as the free metal surface. The fractional coverage θ is equal at the outer surface and the inner interface in the steady state. At the outer surface, the following reaction occurs in pure hydrogen:

$$H_2(g) \underset{d_1}{\overset{c_1}{\rightleftarrows}} 2H_a \tag{27}$$

where (g) refers to gas-phase species and (a) refers to adsorbed species. In the steady state, the coverage is

$$\frac{\theta}{(1-\theta)} = \left(\frac{c_1}{d_1}\right)^{1/2} p_{H_2(g)}{}^{1/2} \tag{28}$$

where θ is the fractional coverage of hydrogen and $p_{H_2(g)}$ is the hydrogen gas pressure. Equation 28 is valid, for both the metal/semiconductor interface and the outer metal surface. The change in the build-in voltage can be written as[130]

$$\Delta V_{bi} = -\mu N_{ads}\theta/\epsilon_S \tag{29}$$

where μ is the dipole moment of an adsorbed hydrogen atom, N_{ads} is the density of adsorption sites, and ϵ_S is the permittivity of the semiconductor. Moreover, the increase of the interfacial charge density causes the change in the ideality factor. The analytical relation between the ideality factor and the interfacial charge density is given by[131]

$$n = 1 + \frac{\Delta}{\epsilon_i}\left(\frac{\epsilon_s}{W} + eN_{ssb}\right) \tag{30}$$

where Δ is the interfacial layer thickness (see Figure 7), ϵ_i and ϵ_s are the permittivities of the interfacial layer and the semiconductor substrate, respectively, W is the depletion layer width, e is the electronic charge, and N_{ssb} (cm^{-2} eV^{-1})[131] is the density of the interface states that are in equilibrium with the semiconductor.

3.5. Extraction of Schottky Diode Parameters for Sensor Applications

3.5.1. Introduction

In Figure 9, a cross section of a typical chemical sensor based on a Schottky junction is shown. Each Schottky barrier diode comprises two contacts, or junction areas, by definition: (1) between metal I and the semiconductor forming the Schottky barrier junction, which is the origin of the sensor signal, and (2) between metal II and the semiconductor forming the ohmic contact, which has to be inactive and, hence, should not contribute to the sensor response. The type of contact is defined by the work function of the materials used for fabrication (see section 3.2.1 and Figure 4). It should be noted that the area of the ohmic contact of the sandwich structure shown in Figure 9 is much larger than that of the Schottky junction, in analogy to auxiliary and working electrodes in electrochemical experiments.

In Figure 10, the schematic band diagram and the equivalent circuit of a chemical sensor based on an ideal Schottky junction device, i.e., without an appreciable interfacial layer or interface states, is shown. The equivalent circuit of the Schottky barrier diode in Figure 10 shows those parts which can be influenced by the chemical interaction of gases with the chemical sensing material: (1) the barrier region (of thickness W_J) formed by metal I and the semiconductor having a capacitance C_J in parallel with the junction resistance R_J, and (2) the neutral bulk (of thickness W_B) of the semiconductor with a bulk capacitance C_B in parallel with the bulk resistance R_B.

Both metal I and the semiconductor, forming the Schottky barrier junction, can be used as the chemical sensing components interacting with gases and vapors. Their choice and combination defines the working principle as well as

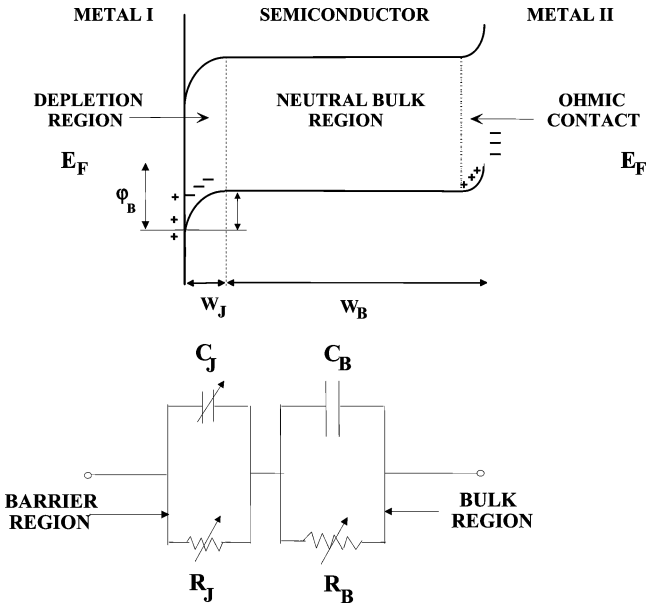

Figure 10. Schematic band diagram and equivalent circuit of an ideal Schottky barrier diode.

the sensitivity and the selectivity of the sensor device. The generation of the "sensor response", i.e., sensor signal, of the Schottky barrier diode is originated in the change of the junction characteristics (i.e., $J-V$ or $C-V$ characteristics) by alternating the Schottky barrier height or the built-in voltage. The response can be due either to *adsorption* of the species of interest at the metal surface affecting interfacial polarization by formation of a dipole layer or to *absorption* of gases or vapors of interest by the semiconductor and their interaction with the semiconductor, which changes its work function and, hence, the contact potential or built-in voltage of the diode. The former is mostly related to Schottky barrier diodes based on inorganic semiconductors and is discussed in section 4.1, whereas the latter is related to Schottky barrier diodes based on organic semiconductors discussed in section 4.2.

It should be noted that the interaction of gases or vapors with the semiconductor, which causes a change of the doping level, leads not only to a change of the work function of the semiconductor, i.e., a change of the junction resistance R_J and the junction capacitance C_J of the Schottky barrier junction, but also to a change of the bulk resistance R_B of the semiconductor (see Figure 10). In this case, the sensor device works as both a junction controlled device, with a diode current in the low bias voltage region exponentially related to the change of the built-in voltage, and a bulk controlled device in the high bias region, with a diode current linearly related to the change in conductivity. The latter represents a simple chemiresistor device. These compensatory effects are discussed in section 4.2.4.3.

In general, the gas sensitivity of diodes is represented by the so-called gas-induced voltage shift, ΔV, extracted from current voltage characteristics and is defined as[29,132]

$$\Delta V = V_{gas} - V_{air} \quad \text{at} \quad J = \text{constant} \tag{31}$$

where V_{gas} and V_{air} are the applied voltages at a constant current density in gas and in air, respectively. In Figure 11 a typical change in the $J-V$ characteristic of a Schottky barrier diode due to interaction with a gas or vapor of interest is shown. ΔV indicates the gas or vapor induced voltage shift

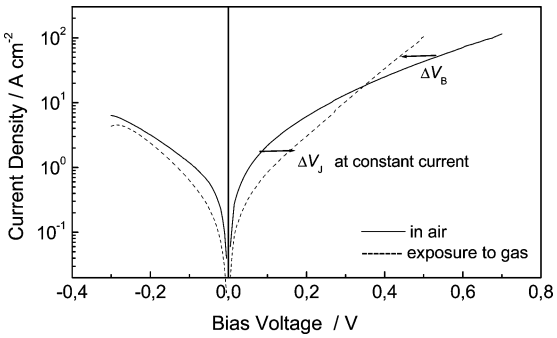

Figure 11. Typical change in the $J-V$ characteristics of a Schottky barrier diode due to interaction with a gas or vapor of interest. ΔV indicates the gas or vapor induced voltage shift at constant current density.

at constant current density. It can be either junction (i.e., ΔV_J) or bulk (i.e., ΔV_B) controlled, as discussed above.

The extraction of the sensing information from Schottky barrier diodes can be done by operation in constant current mode. Hence, the sensor response is the output voltage. Figure 20 shows a typical example of an experimentally obtained transient response of the output voltage of a Schottky barrier diode operated in the constant current mode.

3.5.2. Current–Voltage Characteristic

Taking into account the image force between an electron and the surface of the metal, eq 7 can be rewritten as[82]

$$J_0 = A^{**}T^2 \exp\left[-\frac{\phi_b - \Delta\phi_{bi}}{kT}\right] \tag{32}$$

For metal/semiconductor contacts, the value of J_0 can be readily correlated with a thermodynamic property of the interface, the barrier height of the junction, ϕ_b.

Provided that the current−voltage characteristics are sufficiently close to ideal characteristics to allow a reliable value of J_0 to be determined, the effective barrier height can be deduced in two ways:

(1) If A^{**} is known, the value of J_0, found by extrapolating the straight part of the $\ln\{J/[1 - \exp(-eV/kT)]\}$ vs V plot to $V = 0$ (eq 19), immediately gives the effective barrier height $\phi_e = \phi_b - \Delta\phi_{bi}$. A^{**} is often not known with any great precision, but because an error of a factor of 3 in A^{**} gives rise to an error of about kT/e in ϕ_e, an imprecise value can usually be used unless a very accurate measurement of ϕ_e is required. The determination of the zero-bias barrier height from current−voltage characteristics is only reliable if the semilog plot of J vs V is linear with a low value of n ($1 < n < 1.1$). For large values of n or a nonlinear plot of $\ln J$ as a function of V, the Schottky barrier is far from ideal. This is probably due to the presence of a thick interfacial layer and/or to recombination in the depletion region and/or to tunneling conduction.

(2) If A^{**} is not known, a plot of $\ln(J_0/T^2)$ against T^{-1} should give a straight line of slope $-\phi_e/k$ and intercept on the vertical axis equal to $\ln A^{**}$. This is the most common case for the Schottky diodes based on organic semiconductors, because of the lack of the effective mass of charge carriers. The barrier height is generally a decreasing function of temperature, because the expansion of the lattice causes a change in the band gap. To a first approximation, one can write $\phi e(T) = \phi e(0) - bT$, in which case the method gives the barrier height at absolute zero.

A problem arises if the diode has a large series, i.e., bulk resistance (see Figure 10), or the semiconductor is low doped. This is typical for most polymeric Schottky diodes.[133] The resistance is mainly due to the resistivity of the polymer film. In this case, the region over which the plot of ln J vs V is linear may be small, and accurate extrapolation to zero voltage may be difficult. Moreover, the polymer surface cannot be exposed to any chemical etching process; therefore, it can be expected that irregularities will be brought into contact with the metal and the effective area of the junction will be somewhat uncertain.

To circumvent these difficulties, the use of a Chot plot,[134] which is a modified Norde plot, has been suggested by Inganäs[135] to determine the effective barrier height.

3.5.3. Capacitance–Voltage Characteristic

An independent way to determine the barrier height involves the measurement of the differential capacitance of the Schottky barrier contact. The procedure is known as the Mott−Schottky or capacitance−voltage method. According to the Schottky theory, the depletion layer capacitance (/F·cm^{-2}) of the metal/semiconductor contact

$$C = \frac{\delta Q}{\delta V_r} \tag{33}$$

can be expressed as[81]

$$C^{-2} = \frac{2\left(V_{bi} - V - \frac{kT}{e}\right)}{e\epsilon_S N} \tag{34}$$

where Q is the charge associated with the band bending, V_r is the reverse bias voltage, V is the applied voltage, and N is the free charge carrier concentration. If ϕ_b is independent of V (i.e., if there is no appreciable interfacial layer), a plot of C^{-2} against V (Mott−Schottky plot) should give a straight line with an intercept $-V_I$ on the horizontal axis equal to $-(V_{bi} - kT/e)$. The barrier height is then given by

$$\phi_b = eV_{bi} + \xi = eV_I + kT + \xi \tag{35}$$

The free charge carrier concentration, N, can be determined from the slope of the C^{-2} vs V plot. The depletion layer width, W, is given by

$$W = \left(\frac{2\epsilon_s\phi_{bi}}{eN}\right)^{1/2} \tag{36}$$

If N is not constant, the plot is no longer linear. In this case, the differential capacitance method can be used to determine the doping profile. The derivative of eq 35 gives[81]

$$N = \left(\frac{-2}{e\epsilon_s}\right)\left[\frac{dV}{d}C^2\right] \tag{37}$$

In practice, the junction is reverse polarized, and small oscillations δV are superposed. If no trap exists, the variation of the charge associated with the band bending δQ corresponds to the variation of the free charge carrier concentration at the edge of the depletion zone. If traps exist, they contain part of the charge δQ. To get rid of them, one has to perform measurements at high frequency (>100 kHz).[136] For such a frequency, only the semiconductor depletion charge changes. Another problem then arises: the bulk resistance contribution, which disappears at low frequency. A compromise must be found to minimize these two contributions. This method of barrier height determination is generally straightforward for metal/semiconductor contacts, yielding the flat-band barrier height, which does not include the image force lowering present at the junction. However, when some of the applied voltage is dropped across an interfacial dielectric layer, or when traps are present in an interfacial layer, the capacitance−voltage data will not generally adhere to the simple relationships of eq 33 and eq 34, respectively. Hence, the capacitance method gives results which can differ significantly from those obtained by the current−voltage methods.

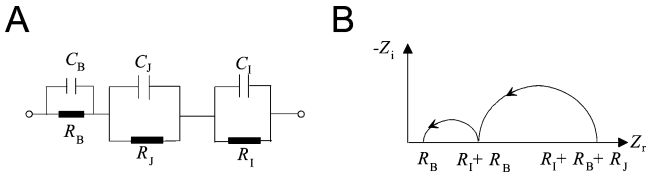

Figure 12. (A) Common equivalent circuit of a Schottky diode junction. (B) Impedance plane plot. Arrows indicate the direction of increasing frequency. The dotted lines imply that the bulk capacitance C_B is often not appreciably distributed.

3.5.4. Impedance Measurement

To gain more insight into the nature of junctions and to obtain the equivalent circuit models for diodes, the complex impedance is usually measured as a function of frequency at different bias voltages.[137] This methodology is analogous to impedance analysis used in electrochemical experiments.

It has been proposed that an ideal Schottky diode (i.e., without an appreciable interfacial layer) can be divided into two regions: (1) the barrier region (of thickness W_J), with a capacitance C_J in parallel with the junction resistance R_J, and (2) the neutral bulk (of thickness W_B), with a bulk capacitance C_B in parallel with the bulk resistance R_B (see Figure 12A).[133]

In most practical metal/semiconductor contacts, the conditions $R_J \gg R_B$, $C_J \gg C_B$, and $\omega_{max}\tau_B \ll 1$ are satisfied.[133,138] The plane plot of the complex impedance is shown in Figure 12B. From Figure 12B, the bulk resistance R_B and the junction resistance R_J can be estimated by the intercepts of the high- and low-frequency extrapolations of the semicircle with the horizontal axis, respectively. Using these values of R_J and R_B, the junction capacitance (for each frequency) and thus the depletion width can be fitted according to

$$Z_r = \frac{R_J}{1 + \omega^2 R_j^2 C_j^2} + \frac{R_B}{1 + \omega^2 R_B^2 C_B^2} \tag{38}$$

$$R_i = -\frac{\omega R_J^2 C_J}{1 + \omega^2 R_J^2 C_J^2} - \frac{\omega R_B^2 C_B}{1 + \omega^2 R_B^2 C_B^2} \tag{39}$$

In most practical metal/semiconductor contacts, the ideal situation shown in Figure 12A is never reached because there is usually a thin insulating layer with a capacitance C_I in parallel with the resistance R_I (see Figure 12B). The insulating layer has three effects:[82] (1) because of the potential drops in the layer, the zero-bias barrier height is lower than it would be in an ideal diode, (2) the electrons have to tunnel through the barrier presented by the insulator so that the current for a given bias is reduced in a manner equivalent to a reduction in the Richardson constant A^{**},

and (3) when a bias is applied, part of the bias voltage is dropped across the insulating layer, so that the barrier height ϕ_b is a function of the bias voltage. This effect changes the shape of the current voltage characteristics of the tunneling current given by[81]

$$J = J_0 \exp\left(\frac{eV}{nkT}\right) \quad \text{for} \quad V \gg \frac{kT}{e} \tag{40}$$

in a manner which can be described in terms of an ideality factor n (greater than unity) defined by eq 41

$$n = \frac{e}{kT}\frac{\delta V}{\delta(\ln J)} \tag{41}$$

4. Schottky Diodes and Their Sensor Applications

4.1. Schottky Diodes Based on Inorganic Semiconductors

In the field of solid-state chemical sensors, Schottky diodes and related devices (MOSFET, MIS structures, etc.) incorporating catalytic metals have been widely studied for their application in the detection of hydrogen and hydrogen-producing compounds.[6] In hydrogen sensors based on Schottky diodes, the key role is played by the Schottky metallization, mostly belonging to the platinum group metals, which ensures the catalytic dissociation of molecular hydrogen into hydrogen atoms (eq 27). It should be noted that the semiconducting substrate is only used to provide sufficiently high Schottky barrier heights, necessary for good sensing performance, but is not the gas-sensitive part of the sensor.

According to the dipole model, originally developed by Lundström,[139] the hydrogen sensitivity of catalytic gate devices is based on the dissociation of hydrogen molecules on the catalytic metal surface and the diffusion through the metal film to form a polarized layer at the metal/insulator interface (see section 3.4.2). The polarized layer gives rise to a shift of the capacitance−voltage ($C-V$) curve of a MOS capacitor or the current−voltage ($J-V$) curve of a Schottky diode. Catalytic gate devices also respond to hydrogen-containing molecules such as hydrocarbons, provided that the molecules are also dissociated on the catalytic metal surface. Oxygen atoms are also dissociated on the catalytic metal surface. Water formation with oxygen atoms from oxygen-containing molecules consumes hydrogen and, therefore, decreases the sensor response. In other words, catalytic metal gates have a direct response to hydrogen and hydrocarbons as well as an indirect response to oxygen molecules, whose effect is to decrease the direct response.

Besides Si, compound semiconductors such as GaAs, InP, SiC, and GaN have been alternatively employed as substrate materials for Schottky diode type hydrogen sensors. Tables 1−3 give an overview of the electrical and gas sensing parameters of the Schottky barrier diodes mentioned above.

4.1.1. Silicon Based Schottky Diodes

From the rapid progress in semiconductor materials and devices, solid-state hydrogen sensors based on the Schottky diode structure with a catalytic palladium metal have attracted intensive interest.[10,140] Silicon based Schottky diodes are inexpensive, and they are compatible with monolithic silicon integrated circuit technology. The measured diode current

Table 1. Electrical Parameters of Schottky Barrier Diodes Based on SiC and Si

structure metal/semiconductor	metal layer[a]	gas/conc	operating temp (°C)	background atmos	sat. current/gas induced sat. current/A	ideality factor/gas induced shift, n/Dn	barrier height/gas induced shift, $\phi_b/\Delta\phi_b$ (eV)	charge carrier density, N_A, N_D (cm^{-3})	ref
Pt/n-SiC	h	NO/10−500 ppm	202−400	synth air		1.73/−0.05	1.33/−0.02 (500 ppm)	1.7×10^{16}	170
Pt/n-SiC	h	H_2/800 ppm	500	synth air	$1.7 \times 10^{-4}/2.1 \times 10^{-4}$	13.5	0.59/−0.005 (800 ppm)		11
Pd/-SiC	h	H_2/800 ppm	400−600	synth air			−/−0.01428 (500 °C)		165
Pt/-SiC	h	CH_4/4800 ppm	400−600	synth air			−/−0.00547 (500 °C)		165
Pt−Pd/(polished)Si	h	NO_2/5−20 ppm NO/50−250 ppm	RT	synth air					140
Pt−Pd/(porous)Si	h	NO_2/5−20 ppm	RT	synth air					140

[a] h = homogeneous.

Table 2. Electrical Parameters of Schottky Barrier Diodes Based on GaAs and AlGaAs

structure metal/semiconductor	metal layer[a]	gas/conc	operating temp (°C)	background atmos	sat. current/gas induced sat. current/A	ideality factor/gas induced shift, $n/\Delta n$	barrier height/gas induced shift, $\phi_b/\Delta\phi_b$ (eV)	charge carrier density, N_A, N_D (cm^{-3})	ref
Pt/n-GaAs	h	H_2/1000 ppm	50−200 °C	synth air			−/−0.19, −0.15	4×10^{14}	7
Pt/n-GaAs	h	H_2/23−1350 ppm	150 °C	synth air/N_2			−/−0.02 (100 ppm, N_2)		8
Pt/n-GaAs	h	H_2/23−1350 ppm	50 °C	synth air/N_2			−/−0.001 (100 ppm, N_2)		8
Pd/n-GaAs	h	H_2/23−1350 ppm	150 °C	synth air/N_2			−/−0.075 (100 ppm, N_2)		8
Pd/n-GaAs	h	H_2/23−1350 ppm	50 °C	synth air/N_2			−/−0.025 (100 ppm, N_2)		8
Pt/n-GaAs	p	NH_3/6−95 ppm	150 °C	synth air/N_2					8
Ir/n-GaAs	p	NH_3/23−1350 ppm	150 °C	synth air/N_2					8
Pt/$Al_{0.3}Ga_{0.9}As$	h	H_2/49−9090 ppm	30−120 °C	synth air			−/−0.074 (9090 ppm)	2×10^{17}	148
Pd/$Al_{0.3}Ga_{0.9}As$	h	H_2/49−9090 ppm	30−120 °C	synth air			−/−0.07 (9090 ppm)	2×10^{17}	148
Pd/n-GaAs	h	H_2/1−5%		synth air			−/−0.28 (5%)	2×10^{17}	147
Au/n-GaAs	p	CO/1−5%	RT	N_2				1×10^{15}	151
Au/n-GaAs	p	NO_2/1−5%	RT	N_2				1×10^{15}	151
Pd/n-GaAs	h	H_2/500−1500 ppm	RT−250 °C	synth air	$6 \times 10^{-10}/9 \times 10^{-9}$ A	1.57/+0.16 (500 ppm)	0.95(RT)/−0.08 (500 ppm)	1×10^{15}	150
Pd/n-GaAs (MOS)	h	H_2/5−5000 ppm	80 °C/110 °C	N_2		1.083/−0.009 (1010 ppm)	0.786/−0.046 (1010 ppm)	1.5×10^{17}	150

Table 3. Electrical Parameters of Schottky Barrier Diodes Based on InP and GaN

structure metal/semiconductor	metal layer[b]	gas/conc	operating temp (°C)	background atmos	sat. current/gas induced sat. current/A	ideality factor/gas induced shift, $n/\Delta n$	barrier height/gas induced shift, $\phi_b/\Delta\phi_b$ (eV)	charge carrier density, N_A, N_D (cm^{-3})	ref
Pd/InP (MOS)	h	H_2/5−5000 ppm	80 °C/110 °C	N_2		1.072/−0.047 (1010 ppm)	0.677/−0.21 (1010 ppm)	1.5×10^{17}	150
Pd/n-InP	h	H_2/100 ppm	RT	synth air	$7.5 \times 10^{-8}/4.3 \times 10^{-6}$	1.8/−0.88	0.72/−0.19 (100 ppm)	10^{16}	10
Pd/n-InP (MOS)	h	H_2/15−1010 ppm	RT−110 °C	synth air			0.63/−0.15 (1010 ppm)	1.5×10^{17}	9
Pd/n-InP	h	H_2/15−1010 ppm	RT−110 °C	synth air			0.42/−0.02 (1010 ppm)	1.5×10^{17}	9
Pd−Ge−Pd/p-InP (pseudojunction)	h	NO_2/10 ppm	RT−100 °C	synth air		1.06/+0.14	0.906/−0.039 (10 ppm)	5×10^{16}	155
Pd*/n-InP[a]	h	H_2/15 ppm−1 vol %	RT−118 °C	synth air	/3.2×10^{-6}	1.12/+2.55	0.588/−0.177 (5000 ppm)	10^{17}	152/153
Pt/AlGaN/GaN	h	CO/8−160 ppm	250−300 °C	synth air			1.01/−0.06 (250 °C, 8 ppm) 1.12/−0.03 (300 °C, 8 ppm)		163
Pt/AlGaN/GaN	h	H_2/5 vol %	200−800 °C	N_2		1.5	−/−0.0114		162
IrPt/AlGaN/GaN	h	H_2/5 vol %	200−800 °C	N_2		1.4	−/−0.0246		162
PdAg/AlGaN/GaN	h	H_2/5 vol %	200−800 °C	N_2		1.6	−/−0.0941		162
Pt/GaN	h	H_2/500−2000 ppm	400 °C	synth air	3.5×10^{-12}	1.37	1.15/−		161

[a] Pd* indicates electroless plated. [b] h = homogeneous.

varies exponentially with the lowering of the hydrogen-induced Schottky barrier height.[141] Therefore, these Schottky diodes often exhibit excellent hydrogen detection sensitivities.

The formation of palladium silicide at the Pd/Si Schottky interface leads to the degradation of detection capacity.[142] An ultrathin (~30 Å) oxide layer introduced into the Pd/Si interface prevents the formation of palladium silicide,[142,143] forming a conducting MIS (metal−insulator−semiconductor) diode. However, the sensitivity toward hydrogen is significantly decreased, if the oxide layer is not properly defined. Therefore, the high quality of the oxide layer is a key factor for the device performance. This certainly increases the fabrication complexity and the cost. In the MIS configuration, the Schottky barrier height of the Pd/Si system is found to depend quite strongly on the Pd effective work function and hence on the hydrogen ambient.

Zhang at al. investigated Pt−Pd/Si−Al Schottky diode structures for detection of NO_2 from 6 to 22 ppm gas concentrations and of NO from 50 to 250 ppm gas concentrations, respectively. The sensor operates at room temperature. The response is roughly proportional to the logarithm of the gas concentration.[140]

Mesoscopic polysilicon wires coated with a thin film of palladium have been used as hydrogen sensors. The wires show an increase in their electrical resistance, when hydrogen reacts with the sensitive layer.[144]

Porous silicon obtained from p+-type silicon wafers were impregnated with Pd nanoparticles using an electroless process. It has been shown that the distribution of nanoparticles over the porous media creates a higher gas sensitivity toward hydrogen.[145]

4.1.2. GaAs Based Schottky Diodes

In a metal/semiconductor junction, the height of the Schottky barrier depends on the work function difference between the metal and the semiconductor according to eq 4. However, as for many III−V semiconductors, the observed value of the barrier height of a metal/GaAs contact does not follow the simple theory in terms of the metal work function and the electron affinity of GaAs due to the high density of surface states, which causes a pinning of the Fermi level. Many models have been developed to explain this discrepancy. Among them, the effective work function model by Freeouf et al.[146] emphasizes the role of the intermediate layer formed by the reaction between the metal and GaAs to determine the barrier height. However, some authors have found evidence of unpinning of the Fermi level in metal/GaAs interfaces fabricated on clean (100) GaAs surfaces. This offered a way to fabricate metal/GaAs Schottky diodes with high sensing capability.[147,148]

Lechuga et al. reported a Pt/GaAs Schottky diode reaching a low detection limit for hydrogen of 6 ppm in nitrogen and 200 ppm in air.[7,8] Liu et al. proposed the fabrication of a planar-type Pd/GaAs Schottky diode as a hydrogen sensor exhibiting an interfacial oxide, which weakens the Fermi level pinning and, hence, improves the barrier height.[149] The use of a porous GaAs semiconductor has been investigated to improve the performance of Schottky diode hydrogen sensors, both in terms of sensitivity and response. Pd/porous-Ga/As and Au/porous-GaAs Schottky junctions have been fabricated, which show sensitivity toward hydrogen and polar gases, e.g., CO, NO, respectively.[150,151] Pd/porous-GaAs Schottky diode gas sensors exhibited large sensitivity of more than three times higher than that of Pd/GaAs contacts with a response time of 1 s toward 500 ppm hydrogen gas. It has been found that this promoting effect could be related to the formation of pore structures (effective adsorption centers) in the Pd contact induced by the porosity of the GaAs wafer.

A urea sensor has been presented using an ammonia gas sensor based on a Pt/GaAs Schottky diode and a urease-immobilized membrane. The authors used discontinuous platinum films which proved to be effective and reliable in solid-state chemical sensors for the detection of NH_3 gas.[8] The Schottky diodes have been coated with an organic layer in order to protect the devices during measurements in solution, as well as to use it as a support for biological material.

4.1.3. InP Based Schottky Diodes

Pd/InP Schottky diodes have been regarded as promising devices for hydrogen sensing.[149,152] At room temperature, it has been found that the Pd/InP Schottky diode exhibits superior sensing performances for the detection of hydrogen. Yousuf et al. demonstrated essentially high hydrogen response in the $J-V$ characteristics of a Pd/InP Schottky diode.[10] Although enormous current variations are observed, the low barrier height associated with the high defect state density at the Pd/InP interface severely restricts the allowable variation in the barrier height. Recently, electroplating techniques have also been proposed to fabricate the Pd/InP Schottky diodes.[153] Although uniformity and adhesion related problems must still be solved compared with traditional vacuum deposition techniques, electrochemical techniques do exhibit the advantages of easy operation, simple equipment, and low cost.[154] Particularly, because of the specificity the low-energy process, the electrochemical techniques can eliminate the Fermi-level pinning effect and lead to well behaved Schottky contact properties, which can remarkably improve the sensing performances of Pd/InP Schottky diodes.

Talazac et al. have presented a different type of Schottky based gas sensor.[155] The detection mechanism is based on the electron exchange of the gaseous molecules with a thin semiconducting layer between the Schottky contact and the semiconducting substrate forming a pseudo-Schottky barrier diode. High sensitivities in the ppb range toward NO_2 and O_3 could be found. However, the sensors suffer from long-term aging effects.

4.1.4. GaN and AlGaN Based Schottky Diodes

GaN and AlGaN are attractive as materials for the fabrication of various chemical and biochemical sensors:[156] the bulk and surface properties are chemically stable due to large band gap energies, the materials allow sensing operation at high temperatures, and the materials are environment friendly.

The Schottky barrier heights are much more dependent on the metal work function[157] than those for other III−V materials, indicating a weaker Fermi level pinning. However, Schottky diodes formed on GaN and AlGaN materials exhibit excess reverse leakage currents, which are many orders of magnitude larger than the prediction of the standard thermionic emission model (see section 3.2.2). Another issue related to the metal/semiconductor interface is a poor ohmic contact. Large leakage currents in Schottky diodes are particularly problematic for constructing high-performance sensors.[158] As a model which explains large leakage currents in nitride-based Schottky barriers, Hasegawa et al. recently

proposed a thin surface barrier model[159] involving donors near the surface. Due to the presence of ionized high-density donors, the width of the Schottky barrier is greatly reduced, and the electrons tunnel through this barrier by the thermionic field emission or the field emission mechanism.

On free surfaces of GaN and AlGaN, high-density surface states exist, which cause charge−discharge transients leading to performance instability, such as current collapse, and poor long-term reliability.

Recently, experimental and theoretical investigations on the role of oxygen impurities in GaN and AlGaN have indicated that oxygen acts as a shallow donor close to the surface with an activation energy of about 30 meV.[160] Therefore, the elimination of oxygen from AlGaN and GaN layers is highly desirable prior to the sensor fabrication in order to realize high-performance sensors, e.g., by using an ultrathin Al layer as a getter material for oxygen.[157]

Schottky diodes on AlGaN/GaN heterostructures with Pt, IrPt, and PdAg catalytic metals have been fabricated and characterized from 200 to 800 °C for hydrogen sensing operation.[161] The hydrogen sensitivity of Pt and IrPt diodes improves with the increase in temperature due to a more effective hydrogen dissociation. The sensitivity of PdAg diodes degrades with increase in temperature due to thermal instability of PdAg.[162]

Schottky gas sensors for CO were fabricated using a Pt-AlGaN/GaN Schottky diode. The CO sensors show good sensitivity in the temperature range 250−300 °C.[163]

4.1.5. SiC Based Schottky Diodes

The operating temperature of gas sensors using silicon substrates is limited below 250 °C due to the small band gap of silicon. This restricts their use in specific environments such as automotive, aeronautical, and environmental areas. Semiconductor substrates with a large energy band gap such as silicon carbide and diamond can be used for sensors operating at high temperatures.

The use of catalytic metal gate SiC devices as gas sensors for hydrogen and hydrocarbons has been extensively investigated by several groups. Janson et al. reviewed the effect of hydrogen on the wide band gap semiconductor SiC and its influence on catalytic metal/SiC Schottky diodes.[164] Kim et al. investigated hydrogen and methane gas sensors using Pt−SiC and Pd/SiC Schottky diodes operating at temperatures in the range 300−500 °C.[11,165]

Annealing effects on Pd/6H-SiC Schottky diodes have also been investigated.[166] The studies indicated that the response of the diode to hydrogen degraded after annealing at 425 °C due to interfacial diffusion of silicon into the Pd film region after dissociation from SiC. Palladium silicides are formed as the major interfacial products. The use of a $Pd_{0.9}Cr_{0.1}$ alloy film deposited on a 6H-SiC epilayer results in Schottky diodes exhibiting a stable catalytic surface and a significant improvement of the device sensitivity.[167]

Some reports deal with the response of catalytic metal gate SiC devices to nitric oxides (NO_x). Zubkans et al.[168] reported the direct response to NO_x, which could be increased after a treatment with ammonia. Katsube et al. showed that thin catalytic metal gate Schottky diodes and p/n heterojunctions on Si substrates can be used for direct NO_x detection at room temperature.[169] They extended their investigations using SiC substrates for high-temperature operation[170] for direct detection of NO_x at elevated temperatures up to 400 °C at minimum concentrations down to 10 ppm. The Langmuir adsorption model can describe the response of these devices.

4.1.6. CdS_xSe_{1-x} Based Schottky Diodes

It has been shown that the bulk photoluminescence of semiconductors can be used to probe the Schottky barrier characteristics of both semiconductor/metal diodes[171] and photoelectrochemical cells.[172] In particular, the electric field in the semiconductor can be estimated from the PL intensity using a dead-layer model: electron−hole (e^-−h^+) pairs, formed within a distance from the interface in the order of the depletion width, do not contribute to the bulk photoluminescence. Schottky diodes have been fabricated with Pd because of the known sensitivity of the current−voltage characteristic to hydrogen. Carpenter et al.[173] showed that, besides the decrease of the Pd work function on exposure to hydrogen, the variation in Schottky barrier height with hydrogen strongly influences the bulk photoluminescence intensity of the Pd/CdS Schottky diode.

The bulk photoluminescence intensity is enhanced upon exposure to hydrogen. In air the bulk photoluminescence intensity of the Schottky diode returns to its original value. The spectral changes are consistent with a reduction in Schottky barrier height resulting from the dissolution of hydrogen in Pd. Qualitatively, the bulk photoluminescence is expected to rise because the smaller electric field in the semiconductor allows a larger fraction of e^-−h^+ pairs to radiatively recombine. By regarding the region supporting the electric field as being completely nonemissive, a quantitative expression for the relative intensity of the bulk photoluminescence can be obtained:

$$\phi_{air}/\phi_{H_2} = \exp(-\alpha\Delta D) \tag{42}$$

where ϕ_{air} and ϕ_{H_2} are the radiative quantum yields in air and in hydrogen, respectively, ΔD is the difference in dead-layer thickness between the two media, and α is the sum of the solid's absorptivities for the exciting and emitted light, respectively. ΔD can be used to calculate the reduction of the Schottky barrier height. By substitution of the depletion width W by ΔD, eq 36 gives the change in barrier height upon exposure to hydrogen.

4.2. Schottky Diodes Based on Organic Semiconductors

Electrical conductivities of organic semiconductors can be varied over the full range from insulator to semiconductor through p-doping or n-doping (see section 2.2). They offer a viable alternative to conventional inorganic semiconductors in many applications because of their unusual electrical properties, diversity, ease of fabrication, large area, and potentially low cost. Much research has been carried out on the use of organic semiconductors as active materials in electronic devices. Fabrication of electronic devices, such as OFETs, OLEDs, and devices based on Schottky barriers is the most important application of these materials.

The use of different semiconducting organic films for the detection of gas and vapors has been reported by a number of groups.[27−30,174] Whereas the chemical stability in a given temperature range and in ambient environment is a basic requirement of organic semiconductors to be used as active material in electronic devices, the modulation of physical properties of the organic semiconductors as a function of gas or vapor concentration is a prerequisite to be used as

Table 4. Parameters of Molecular Semiconductor Schottky Barrier Diodes Based on Phthalocyanines (Pc)

device config		doping	barrier height ϕ_b/eV	charge carrier density N_s/cm^{-3}	depletion width W/ nm	charge carrier mobility μ /m^2 V^{-1} s^{-1}	ref
Au/AlPcCl/Al	p-type	oxygen	1.03	1.7×10^{19}		1.73×10^{-8}	194
	p-type	as deposited	1.09	7.5×10^{18}		1.58×10^{-8}	
ITO/AlPcCl/Al	p-type	oxygen	0.65	2.2×10^{17}		1.2×10^{-6}	196
Au/FePcCl/Au	p-type			5.1×10^{18}			193
Au/TiOPc/HOPG	p-type	oxygen		1.6×10^{18}			105
	n-type	as deposited		3.4×10^{17}			
Au/NiPc/Al		oxygen	1.2	1.1×10^{16}	169	5.8×10^{-6}	176

Table 5. Electrical Parameters of Polymer Schottky Barrier Diodes Based on Polythiophene (PT), Poly(3-alkylthiophenes) (P3AT)[a], Polyanilines (PANI), and Polypyrroles (PPy)[a]

structure	doping agent	ideality factor n	contact or built-in potential ϕ_{bi}/eV	barrier height ϕ_b/eV	charge carrier density N_A/cm^{-3}	ref
			Polythiophenes—*PT*			
Al/PT/Au	ClO_4	13.0	0.38	0.66		211
Al/P3DT/Au−Sn	undoped			0.4	3.0×10^{14}	217
Al/P3HT/Au	undoped	3.9			1.0×10^{17}	91
Al/P3HT/ITO	PF_6			0.34		205
Al/P3MeT/Pt	reduced	3.0	0.35	0.75	3.5×10^{15}	216
Al/P3MeT/Au	BF_4	4.5	1.2	1.5	6.4×10^{19}	239
	reduced	2.5	0.6	0.8	4.6×10^{16}	239
	PF_6			0.45		205
Al/P3OT/ITO	undoped	6.1		1.01	2.9×10^{17}	205
	$FeCl_3$	4.9	0.52	0.72	7.0×10^{16}	203
Al/P3OT/Au	undoped	1.2	0.7			204
			Polyanilines—*Pani*			
Al/Pani/Au	HCl	1.24		0.38		222
	TOS	1.3	0.72	0.78	2.8×10^{18}	220
	PAA	1.7	0.82	0.87	1.4×10^{18}	
	undoped	1.95	0.9	1.03	1.8×10^{17}	
Al/Pani[b]/Au	HCl	1.46−1.64		0.33−0.41		222
Al/Pani/ITO	HCl	4.2	0.65	0.76	3.1×10^{17}	228
In/Pani/Pt	DBS/HCl	3.12	0.69	0.803	3.06×10^{17}	221
			Polypyrroles—*PPy*			
Al/PPy/Au	BF_4	4−7	∼0.7	0.7−0.76	1.0×10^{22}	185
Al/PPy−NMPy/Au	BF_4	1.4−2	0.78−0.82	0.7	10^{16}−10^{17}	185
In/PPy−NMPy/Au	ClO_4	1.2	0.23	0.81	7.0×10^{17}	182
Au/PPy/Pt	CuPcTS	3.6	0.26	0.63	1.2×10^{20}	186
	PbPcTS	3.8	0.24		4.6×10^{19}	
	NiPcTS	4.0	0.23		3.7×10^{19}	
	CoPcTS	4.2	0.2		1.9×10^{19}	

[a] ClO_4 = perchlorate; CuPcTS = copper phthalocyanine tetrasulfonate; PbPcTS = lead phthalocyanine tetrasulfonate; NiPcTS = nickel phthalocyanine tetrasulfonate; CoPcTS = cobalt phthalocyanine tetrasulfonate; DBS = dodecylbenzenesulfonic acid; D = dodecyl; O = octyl; M = methyl; H = hexyl; NMPy = *N*-methylpyrrole. [b] Modified with metal−2.5-diaminobenzenesulfonic acid.

the sensing element in chemical sensors. However, the details of the gas response mechanism have not been completely elucidated. From a practical point of view, the gas sensing characteristic is strongly influenced by a number of processing parameters: for example, the growth rate, the thermal annealing,[29] the polymerization temperature,[175] and the nature of the dopants.[132] By exposure of the polymers to certain gaseous species exhibiting electron donor or acceptor behavior,[176,177] the Fermi level position is changed by either increasing or decreasing the doping level according to section 3.4.1. In this case, a gas-induced change of the Schottky diode barrier characteristic can be observed. Furthermore, the increase or decrease in the ideality factor during gas/polymer interactions, which is due to a generation or reduction of the interface state density, can influence the gas sensitivity of the junction as well.

Despite these advances in the use of chemical sensing applications, the detailed properties and roles of interfaces in organic semiconductor devices remain elusive. Parker suggests that charge injection into organic materials proceeds via tunneling across interfacial barriers.[178] Improvement of device performance through interface modification has also been reported.[179] Up to now, most Schottky diodes based on organic semiconductors were fabricated and characterized using metals with low work function, such as Al, In, or Ca.[27,180−182,217] These diodes show unstable electrical and chemical sensing properties, which have been attributed to the high chemical reactivity of the metal used.[183] The nature of the interfacial layer between these metals and the semiconducting polymers is commonly difficult to define.[181]

In Tables 4−7, diode parameters of organic Schottky diodes are given. The data show that, unlike the case of conventional metal/semiconductor contacts, the electrical properties of contacts based on organic semiconductors can be manipulated not only through the choice of materials, methods, and conditions of preparation but also through the type of dopants incorporated into the organic semiconductor (see section 2.2). This can be exploited to tune the diode characteristics in a definite way. On the other hand, a careful control of the preparation parameters is necessary to obtain reproducible results.

The choice of the metal forming the ohmic contact depends on the work function of the organic material used. For the commonly used polymer-based diodes, consisting

Table 6. Electrical Parameters of PPy-MPcTS Schottky Barrier Diodes Extracted from *J*−*V* and *C*−*V* Characteristics, Measured in Air and Exposed to 11 pm NO_2

	saturation current density J_0/A cm^{-2}		ideality factor n		rectification ratio (at $\|V\| = 1$ V)		built-in voltage V_{bi}/V	
dopant	air	NO_x	air	NO_x	air	NO_x	air	NO_x
CuPcTS	8.1×10^{-4}	7.0×10^{-5}	3.6	3.2	7.2	13.5	0.26	0.29
PbPcTS	1.5×10^{-3}	7.9×10^{-4}	3.8	3.5	5.2	8.7	0.24	0.27
NiPcTS	6.5×10^{-3}	2.4×10^{-3}	4.0	3.7	3.7	5.1	0.23	0.26
CoPcTS	1.0×10^{-2}	4.8×10^{-3}	4.2	3.8	3.2	4.7	0.20	0.22
TOS	2.5×10^{-2}	1.1×10^{-2}	4.9	4.3	2.1	2.9	0.15	0.17

Table 7. Electrical Parameters of PPy-MPcTS Schottky Barrier Diodes Extracted from *J*−*V* and *C*−*V* Characteristics: Change of NO_2 Sensitivity for Different Polymerization Temperatures of PPy, Measured in Air and in 11 pm NO_2

polymerization temp/K	rectification ratio at $\|V\| = 0.9$ V	saturation current density J_0/A cm^{-2}	ideality factor n	charge carrier conc $N_A/10^{19}$ cm^{-3}
278	2.1	3.1×10^{-2}	4	97.5
283	3	6.3×10^{-3}	3.7	52.6
288	5	1.9×10^{-3}	3.4	37.1
293	6.3	7.9×10^{-4}	3.6	12
303	27.3	1.2×10^{-4}	3.3	2.1
313	156	7.6×10^{-5}	3.1	0.82
323	307	5×10^{-5}	2.5	0.37
333	68	1×10^{-4}	2.9	1.4

of poly(3-octylthiophene),[27] poly(3-methylthiophene),[184] and PPy,[29,185,186] gold was used to form an ohmic contact. The work function of gold has been assumed to be about 5.1 eV. Several studies show that the work function of π-conjugated polymer films is about 5 eV, depending upon the dopant type and the doping level.[64,126] In this case, the barrier between the p-type polymer and gold is relatively small but is predicted to be negative, representing a quasi-ohmic contact, with a symmetric current−voltage dependence. Nevertheless, the experimental contacts are sometimes rectifying,[133] indicating a higher work function of the polymer than that of gold. Hence, the junction characteristics of the ohmic gold/polymer barrier are strongly influenced by the gas sensing behavior of the polymer layer, exhibiting either symmetric or a non-ohmic, i.e., asymmetric, current−voltage characteristics. To overcome this uncertainty, platinum is recommended as metal to form an ohmic contact with the doped p-type conducting polymers.

4.2.1. Phthalocyanines

Phthalocyanines (Pc) are a class of organic compounds of high thermal and chemical stability, which are classified as p-type semiconductors characterized by a low mobility and low charge carrier concentration.[187] They have potential advantages for use as active layers in electroluminescent,[188] photovoltaic,[189] and gas sensor devices,[190] because they are easily processable in low cost and large area device fabrication.[191]

However, it is known that oxygen profoundly influences the electrical properties of phthalocyanines. It has been demonstrated that the dark rectification ratio of Au/Pc/M (M = Au, Cu, Cr, Al) is related to the presence of O_2.[192,193] When the devices are made and studied under vacuum, no rectifying effect is observed. However, by exposure to air, a strong rectifying effect has been found. Acceptor levels are generated within the band gap of these materials in the presence of O_2, and hence, their thermal activation energy is lowered and the conductivity is enhanced.[192,194]

Besides O_2, any other electron acceptors, such as NO_x and Cl_2, induce acceptor levels, while electron donors, such as H_2 or NH_3, remove them. Both change the Schottky diode characteristics.

With most of the phthalocyanines, gold is found to form the ohmic contact,[14,15] and aluminum is found to form the blocking contact.[192,195] Under forward bias, oxygen-doped phthalocyanine thin films show ohmic conduction at low voltages and space charge limited conduction controlled by an exponential distribution of traps above the valence band edge at higher voltages.[192,194,196]

As already discussed above, almost all phthalocyanines show excellent gas-sensing properties for both electron acceptors, such as NO_x,[197−199] HCl,[197] Cl_2[200] and electron donors, such as H_2 or NH_3.[105] The change in the doping level induces a Fermi level shift and a change in the Schottky barrier height. It is supposed that a charge-transfer complex[128] between the organic semiconductor and the gas or vapor is formed during the interaction. Spectroscopic investigations show the accumulation of the gas species in the bulk of the sensitive film and the formation of organic radical cations.[197,201]

Studies of phthalocyanines indicated that the sensitivity and selectivity of the sensor device are strongly influenced by the nature of the central metal ion and also by the crystal structure and/or crystallinity. Nieuwenhiuzen et al.[202] reported that the sensitivities for detection of NO_x decrease in the order Co > Cu > Pb > H > Fe > Mg > Ni, whereas the sensitivities toward NH_3 decrease in the order Pb ≫ Fe > Cu > Ni > Mg. Pc films either prepared by spin-coating or by vacuum deposition show a detection range of 0.3−200 ppm for NO_2[197,202] and one of 1−200 ppm for NH_3[202] without further annealing after film formation. Independent of the central metal ion, phthalocyanines show no sensitivity toward CO, CO_2, CH_4, C_6H_{14}, C_7H_8, SO_2, H_2O, and H_2S.[202] High stability and reproducibility are observed in the sensing behavior of all phthalocyanines, with the exception of PbPc and FePc. Both show a deformation during exposure to NH_3 and NO_2, respectively. Additionally, the crystal structure and size have been shown to vary with operating time.[198,202] The presence of disordered phases between the PbPc particles reduces the response and recovery times during the gas interaction. It was concluded by Sadaoka et al. that the gas-sensing properties of PbPc can be improved by annealing the Pc films at 300 °C in order to form a homogeneous layer of triclinic crystals with a mean diameter less than 0.2 μm.[198]

4.2.2. Polythiophene/Poly(3-alkylthiophenes)

For more than one decade, polythiophene and its derivates have been the subject of intensive experimental and theoretical work.[203−205] Polythiophene and its 3-methyl derivative exhibit a poor processability due to their insolubility. The available materials have not been of the high electronic

quality necessary to use them in electronic devices. In 1986, poly(3-alkylthiophenes) with an alkyl group of more than four carbon atoms became available.[206] They are soluble in several organic solvents and even fusible, which makes them attractive for use in electronic devices ranging from field-effect transistors[207] and light emitting diodes[208] to nonlinear optoelectronic components.[209]

Sundberg et al. investigated the manufacture of metal/polymer contacts.[210] The comparison of the current−voltage and capacitance−voltage characteristics of melt-processed and sputtering-processed devices shows no significant difference between these structures. Both processes influence the polymer surface. The sputtering involves some relatively high-energy particles impinging on the polymer surface, whereas melt-processing can give rise to surface modifications and, hence, to a stronger enhancement of the doping concentration close to the interface than obtained for sputtering. For both devices, $C-V$ characteristics indicate an additional constant capacitance in series with the variable space−charge capacitance of the polymer, which is assigned to an insulating oxide layer at the metal/polymer junction. In the melt-processed device, this layer is probably thicker because the aluminum is exposed to air before making the contact. Similar results were obtained when the rectifying contact was formed by pressing aluminum on the polymer surface.[211] In this context, it should be taken into account that reactive metals such as Al and In might form a thin insulating interfacial oxide layer and probably react with the dopants.[212] This would lead to a lower accumulation of the dopant species at the interface and a wider barrier.

Lous et al. investigated Schottky contacts on highly doped organic semiconductors based on thiophene oligomer by current−voltage and capacitance−voltage measurements.[213] The Schottky diodes obtain their rectifying behavior from a partly undoped p^- layer at the metal/oligomer interface with respect to the higher doped p^+ bulk layer. This low conductive p^- layer implies a large electric field at the interface which can cause a substantial lowering of the Schottky barrier.

Schottky diodes with poly(3-octylthiophene) as the semiconductor and aluminum- and indium-doped tin oxide as the rectifying and ohmic contact, respectively, show a rectification ratio up to 3−4 orders of magnitude. The shape of the $J-V$ characteristics, the high value of the ideality factor, and the observation of series resistance indicate an interfacial layer at the aluminum/polymer interface and the effects of trapping in a region adjacent to the metal.[214]

The effect of oxygen is reversible on structures based on poly(3-methylthiophene).[215,216] The effect of various atmospheres on the electrical characteristics of Mo/poly(3-methylthiophene) Schottky barrier diodes was investigated by Tagmouti et al.[216] The electrical characteristics were mainly affected by the presence of water vapor and oxygen. The capacitance shows a frequency dispersion, which is characteristic for the presence of deep traps induced by oxygen forming acceptor states in the band gap. The authors concluded that oxygen fills the traps and dopes the polymer. The effect of water vapor is manifest by reduction in dopant density and a filling of deep traps, which is irreversible.

Gas-sensitive characteristics toward water vapor, chloroform, and ethanol were observed in poly(3-dodecylthiophene) Schottky diodes.[217] The two types of gases have opposite effects on the diode characteristics; one type (water vapor) increases and the other type (chloroform and ethanol) decreases the reverse bias current. The results were explained by the acceptor and donor behavior, respectively, which results in a change in the Schottky barrier height by doping or undoping of impurity levels in the band gap of the p-type semiconductor.

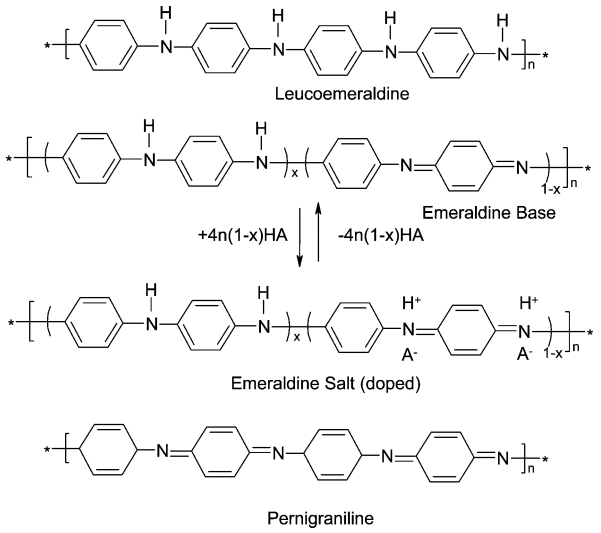

Figure 13. Chemical structure of polyaniline, showing three different oxidation states.

4.2.3. Polyanilines

The advantages of polyaniline compared with other conducting polymers are the easy and cheap oxidative synthesis, the thermal and environmental stability, and the simple nonredox doping in protic acids.[218] Polyaniline is a p-type organic semiconductor, and it can exist in several oxidation states, ranging from fully reduced leucoemeraldine over intermediate and moderately oxidized (doped) emeraldine to the fully oxidized pernigraniline, as named by Green and Woodhead[219] (Figure 13). Acid-doping of the soluble emeraldine base, using organic and inorganic acids, leads to the insoluble highly conducting emeraldine salt.

Schottky diodes have been prepared using either casting[220,221] or electrochemical techniques.[222,223,228] The polymers investigated involve undoped and acid-doped polyanilines, which behave as p-type semiconductors. The diodes, in which aluminum was used as low work function metal to form a Schottky junction, exhibit a moderate rectifying behavior and low leakage current. The values of ideality factor n lie between 1 and 2, indicating either a recombination process in the barrier or a thin insulating layer at the interface. The acid-doping of polyaniline, e.g., with toluene-4-sulfonic acid, can cause a higher rectifying effect and photovoltaic conversion efficiency.

Calderone et al. investigated the metal/polymer interface theoretically, focusing on the interaction between aluminum and the fully reduced form of polyaniline, i.e., leucoemeraldine.[224] The study obtained for the model system Al/p-phenylenediamine indicated that an electron charge is transferred from the metal to the organic system, and the π-electronic levels are strongly perturbed. These results are considered as the basis of the Al/leucoemeraldine interaction.

Chemical sensitivities toward gases and vapors, such as ammonia,[225] hydrogen cyanide,[226] hydrogen,[227] and methane,[228] have been shown. Campos used a sandwich type device based on Al/polyaniline as a sensor for the detection of methane gas. HCl-doped polyaniline was electrochemi-

cally deposited on an indium tin oxide coated glass electrode, which serves as the ohmic contact metal in the Schottky diode. Methane decreased the forward and reverse bias current, indicating an increase in the barrier height.

4.2.4. Polypyrrole

4.2.4.1. General Aspects. Among various conducting polymers, polypyrrole (PPy) has been extensively investigated because of properties that are attractive from the practical point of view: that is, relatively good environmental stability, high conductivity, and ease of preparation either by chemical or electrochemical methods, as well as the possibility of forming homopolymers or composites with optimal properties. A general difficulty of the reproducible PPy preparation arises from its complexity. The structure and hence the properties of the resulting PPy are strongly influenced by a number of variables, e.g., the polymerization potential, the monomer concentration, and the preparation temperature,[229] which are not perfectly controllable. Therefore, the results on PPy vary widely. Two basic methods are used for the preparation of PPy: chemical and electrochemical synthesis. Anions, present in the polymerization solution, are simultaneously incorporated into the polymer as dopants. The final polymer chain bears a charge of unity for every three or four pyrrole rings, which is counterbalanced by the dopant anion.[229] A lot of work has been carried out in order to improve both the chemical and electrochemical synthesis of pyrrole, as reviewed by Rodríguez et al.[229]

There exists a huge number of publications dealing with parameters influencing the final properties of PPy samples during the synthesis. Only some important parameters are briefly discussed below.

The *counterion* is indispensable for the charge compensation of PPy; at the same time the size, shape and structure of the counterion are expected to influence the electrical conductivity. There are a large number of reports comparing the conductivity values of PPy containing aromatic sulfonate anion, such as *p*-toluene sulfonates, aromatic carboxylates, etc., and inorganic anions, such as BF_4^-, Cl^-, ClO_4^-, SO_4^{2-}, etc., and it was found that conductivity was always higher in the case of aromatic dopants.[230]

Few studies have dealt with PPy containing anionic transition-metal complexes, e.g., tetrasulfonated metallophthalocyanines (MPcTS).[231,232] Saunders et al.[231] have studied the physical and spectroscopic properties of PPy-MPcTS (M = Co, Cu, Fe, and Ni) prepared using both aqueous and nonaqueous solution. The conductivities of these materials were found to rapidly decrease upon exposure to air. As a reason for this, it was suggested[67] that the large size of the MPcTS counteranions produced packing inconsistencies within PPy-MPcTS, which facilitates the chemical attack of the polymer backbone by atmospheric oxygen. Walton et al.[232] have studied a competitive doping of PPy during polymerization in an aqueous and acetonitrile solution of ClO_4^- and copper phthalocyanine tetrasulfonate.

The effect of *temperature* on the polymerization process has been studied. It has been shown that the temperature has a significant effect on the conductivity of PPy depending on the combination of solvent and dopant. Toluensulfonate- and perchlorate-doped PPy films, deposited at a lower temperature (280 K) in water, exhibit higher conductivities than films prepared at 293 or 313 K.[229] The authors found that an increase in the temperature favors the polymer growth, which has been related to an overpotential decrease.

4.2.4.2. Metal/Polymer Interface. The polypyrrole family of polymers is a promising candidate for device fabrication because of its relatively high stability in ambient air. Oxidized (p-type) PPy is reported to have a work function close to 5 eV.[122] From theoretical considerations, therefore, the junctions between PPy and metals with low work functions are expected to form a Schottky barrier. Several reports are available on metal/PPy junctions.[182,233,235] Almost all of the results were explained on the basis of the Richardson equation, eq 6.

The high charge carrier concentration found in doped PPy ($N_A \sim 10^{22}$ cm^{-3} assuming that all dopant charges give rise to one hole polaron or half a bipolaron) results in the formation of a very thin Schottky barrier with a narrow depletion width ($\sim$ 10 Å), which may be the reason for the bad rectifying behavior of the polymer Schottky junction due to the dominant tunneling process of the charge carrier transport mechanism (see section 3.2.4). It has been suggested that the introduction of N-substituted pyrroles to PPy lowers the conductivity of the homopolymer.[234] The relationship between the density of dopants and the conductivity has led to investigations of the rectifying characteristics of various copolymers having pyrrole and *N*-methylpyrrole units. The introduction of *N*-methylpyrrole would less influence the delocalization of π-electrons along the polymer chain than that of other N-substituted pyrroles. Schottky junction devices from a pyrrole/*N*-methylpyrrole copolymer have been fabricated exhibiting a relatively low charge carrier concentration of $N_A \sim 10^{17}$ cm^{-3} and a conductivity of $10^{-2}-10^{-4}$ S cm^{-1}.[182,185] The values of the ideality factor (n = 1.20−1.38) are closer to that of an ideal diode, and the rectification ratio is relatively high.

In or Al have mostly been used as low work function metals to from a non-ohmic Schottky barrier with PPy.[137,181−183,233] Gupta et al. reported leaky Schottky barriers of reactive metals, such as Al and In, with the polymer.[233] Some authors concluded that the formation of metal salts at the metal/polymer junction as a result of reaction between the dopant anion and the low work function metal leads to insulating interphases.[137] Other reports show that the ambient (i.e., oxygen) influences the current−voltage characteristics of contacts between these metals and PPy and that the observed hindrance of charge transport was due to the formation of insulating metal oxides.[181,183,235,236] The thin insulating layer at the interface between the metal and the polymer was assumed to be the reason for the anomalous $J-V$ characteristics with a small plateau at low forward bias.[217,237,238] The forward characteristics of this type are comparable with nonequilibrium effects in MIS diodes.[237] Taylor et al. noted that this effect could be further produced when the polymer Schottky diode comprising an aluminum rectifying contact was given a thermal post-metal annealing in air.[239]

On the other hand, it has been shown by Nguyen et al. that a metal with a high work function (e.g., gold) can be used to form a non-ohmic contact with PPy when metal phthalocyanine tetrasulfonates (MPcTS) are used as dopants.[132] These contacts show an exponential and asymmetrical behavior of the $J-V$ curves (Figure 14).

As can be seen in Table 4 and Figure 14, the junction parameters of Au/PPy-MPcTs diodes are strongly influenced by the type of dopant. The junction between PPy-TOS and Au shows a low rectifying ratio and a relatively high saturation current density. This junction seems to be practi-

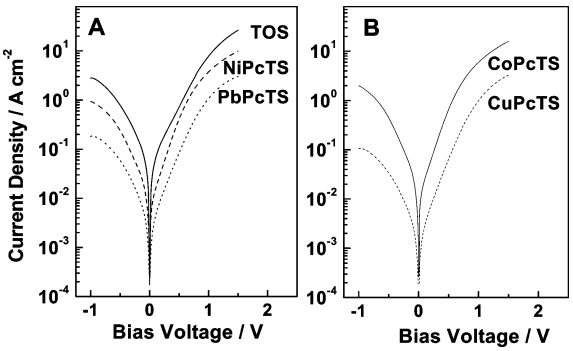

Figure 14. Dark current density vs applied voltage ($J-V$) characteristics of Au/PPy Schottky barrier diodes doped with different dopants.

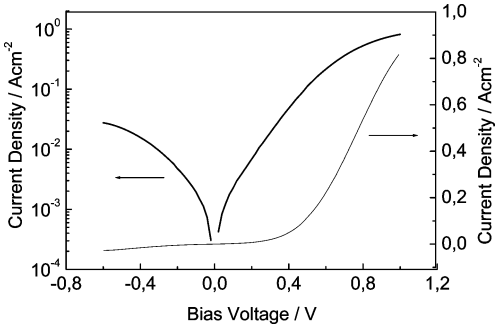

Figure 15. Dark current density vs applied voltage ($J-V$) characteristics of a Au/PPy-CuPcTS Schottky barrier diode.

cally quasi-ohmic. The most optimal diode parameters, such as the rectifying ratio and the ideality factor, were found for the Au/PPy-CuPcTS junction (Figure 15).

The rectification ratios (forward bias current/reverse bias current at 0.6 V) were observed to be between 7.7 and 3.2. The values are slightly larger than that of the Schottky diode based on *trans*-polyacetylene and Pb ($n = 1.5$) reported by Kanicki,[133] and are in good agreement with that for Ti/PPy ($n = 10$) reported by Gupta et al.[240] and for Al/PPy Schottky diodes ($n = 6$) reported by Bantikassegn et al.[137]

Impedance and capacitance measurements give insight into the nature of the diode junctions and the physical properties of PPy as an organic semiconductor.[132] Figure 16 shows the plane plot of the complex impedance of a Au/PPy-CuPcTS Schottky barrier diode, measured at zero bias. The device shows only a single semicircular arc. The experimental curve can be fitted well by applying the equivalent circuit of the diode shown in Figure 16. This indicates the formation of a negligible small insulating interfacial layer (see Figure 7A).

The capacitance−bias voltage curve shown in Figure 17 indicates the formation of a Schottky junction[135] and allows the use of the simple depletion layer theory as already discussed in section 3.5.3. Nguyen et al.[132] determined a value of 0.26 V for the built-in voltage V_{bi} and a charge carrier concentration N_A (concentration of polarons and/or bipolarons) of 1.2×10^{20} cm^{-3} for the CuPcTS-doped PPy layer of 120 nm in thickness. This is in good agreement with $N_A = 1.5 \times 10^{20}$ cm^{-3}, reported by Gupta[233] for electrochemically prepared PPy of 3 μm in thickness, doped with tetrafluoroborate anion.

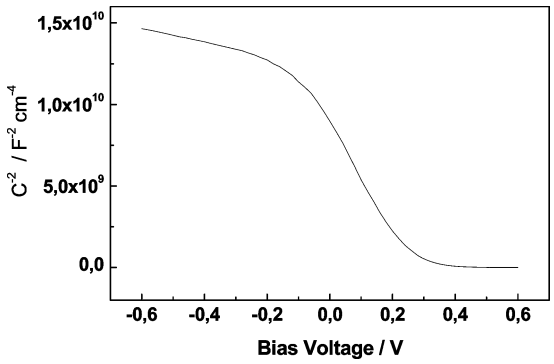

Figure 17. Mott−Schottky plot (C^{-2} vs bias voltage) for a Au/PPy-CuPcTS Schottky barrier diode.

The charge carrier concentration can also be estimated from the doping level, determined by electrochemical quartz microbalance (EQCM) measurements.[241] A doping level of 30.2% is deduced, and a charge carrier concentration of about 3.3×10^{21} cm^{-3} is expected. This value is in accordance with that reported by Buhks et al.[242] (about 3×10^{21} cm^{-3}). It can be seen that the acceptor concentration calculated from capacitance measurements is far different from that estimated from the doping level obtained from the EQCM measurements. This may be due to the large concentration of defects present in PPy that strongly influence the conjugation lengths of the polymer chain[231] (see section 4.2.6.1).

4.2.4.3. Chemical Sensing Properties. *Influence of Dopants.* Several authors,[64,121,243] have reported that the sensitivity of PPy to certain vapors or gases changes with the doping anion. Sensitivities toward organic vapors, such as alcohols, chlorinated hydrocarbons,[121,244] aromatic hydrocarbons,[245] nitrogen oxide gases, and organophosphorous compounds,[121] have been reported. The influence of different metal phthalocyanines incorporated in PPy on the NO_x sensing properties of the Au/PPy diodes has been studied.[121] NO_x exhibits a strong electron acceptor effect on PPy when doped with metal phthalocyanines.[27,29,64] Nguyen at al.

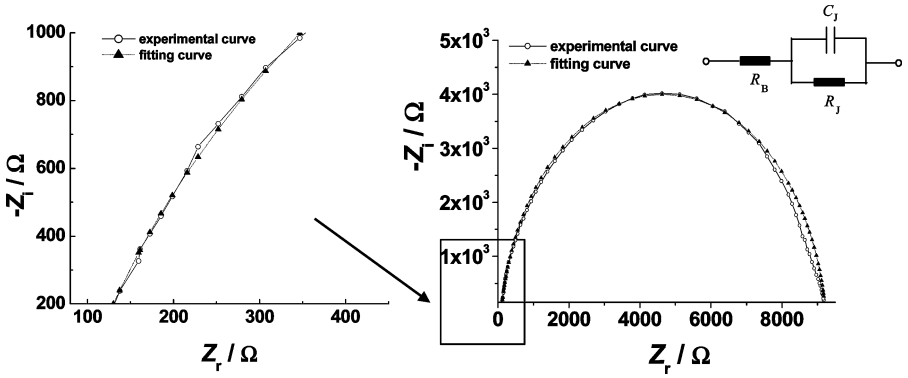

Figure 16. Complex impedance plane plots of a Au/PPy-CuPcTS Schottky barrier diode at zero bias, and a complex plane model.

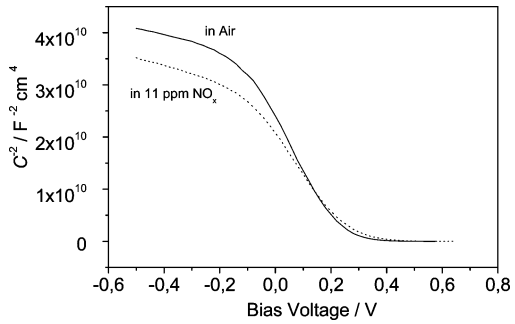

Figure 18. Mott−Schottky plot (C^{-2} vs bias voltage) for a Au/PPy-CuPcTS Schottky barrier diode measured in air and in 11 ppm NO_x.

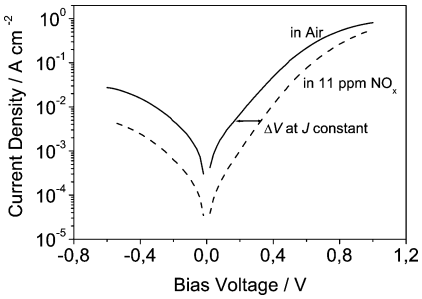

Figure 19. Change in $J-V$ characteristics of Au/PPy-CuPcTS measured in air and in 11 ppm NO_x. ΔV indicates the NO_x induced voltage shift at constant current density.

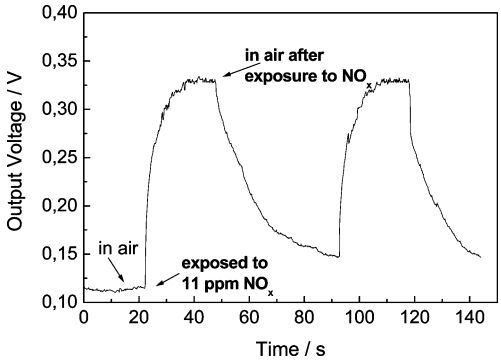

Figure 20. Response curve of a Au/PPy Schottky barrier sensor toward exposure to NO_x by applying a constant current density ($J = 2 \times 10^{-3}$ A cm^{-2}).

showed that the exposure of a Schottky diode with PPy as the semiconducting organic layer to NO_x causes an increase in the doping level of PPy. This leads to a positive shift of its Fermi level and, therefore, increases the built-in potential at the Au/PPy junction.[132] This effect could be confirmed by capacitance voltage measurements (Figure 18).

The change in the $J-V$ characteristics is shown in Figure 19 for the same measurement. The gas sensitivity of the diodes is represented by the so-called gas-induced voltage shift, ΔV, at a constant current density in gas and in air, respectively, which was extracted from current voltage characteristics as discussed in section 3.5.1.

Figure 20 shows the transient response of the output voltage of a Au/PPy-CuPcTS Schottky barrier diode to exposure to NO_x, measured at constant current density.

As already discussed in section 3.5.1, an ideal Schottky barrier diode (i.e., without an appreciable interfacial layer) can be divided into two regions: (1) the barrier region (of thickness W_J), having a capacitance C_J in parallel with the junction resistance R_J, and (2) the neutral bulk (of thickness W_B), with a bulk capacitance C_B in parallel with the bulk resistance R_B.

The NO_x exposure can lead to an increase in the built-in voltage V_{bi} and the depletion width W_J; hence, the resistance R_J of the barrier region can increase as well. In contrast, NO_x exposure may cause a decrease in the bulk resistance R_B of the PPy layer because of the strong acceptor behavior of NO_x. These effects have been confirmed by impedance measurements.[132]

Figure 21 shows the plane plot of the complex impedance of the Au/PPy-CuPcTS Schottky barrier diode, measured in air and in NO_x after different time intervals. It can be clearly seen that when the diode is exposed to NO_x, the bulk resistance decreases and the junction resistance simultaneously increases.

A combination of those compensatory effect can decrease the gas sensitivity of the Schottky barrier diodes. In the low bias region, the junction voltage increases slightly due to NO_x-exposure, while in the high bias region it increases largely. This suggests a large change in the interface layer resistance upon NO_x-exposure, which has been assumed to play an important role in the charge carrier transport across the Schottky barrier.[82]

The change of the diode parameters extracted from current voltage measurements of PPy-MPcTS Schottky diodes exposed to NO_x is listed in Table 6. For comparison, the sensitivity of a PPy-TOS Schottky diode is included. The data listed in Table 6 show that the NO_x sensitivity is strongly influenced by the nature of the dopants. A lower saturation current density is accompanied by a higher rectification ratio and by a lower value of the ideality factor, which are related to a larger value of the NO_x-induced voltage shift measured in the low bias range ($V_{bias} < 0.3$ V). The ideality factor shows a tendency to decrease when the diode is exposed to NO_x. It has been reported by Bardeen[246] that the discrepancy between the real Schottky diode and the ideal may be due

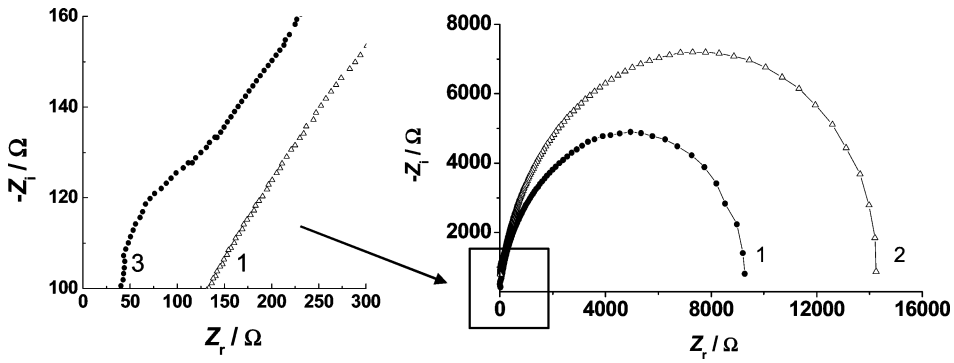

Figure 21. Plane plots of complex impedance of a Au/PPy-CuPcTS Schottky barrier diode (1) in air, (2) and (3) in 11 ppm NO_x.

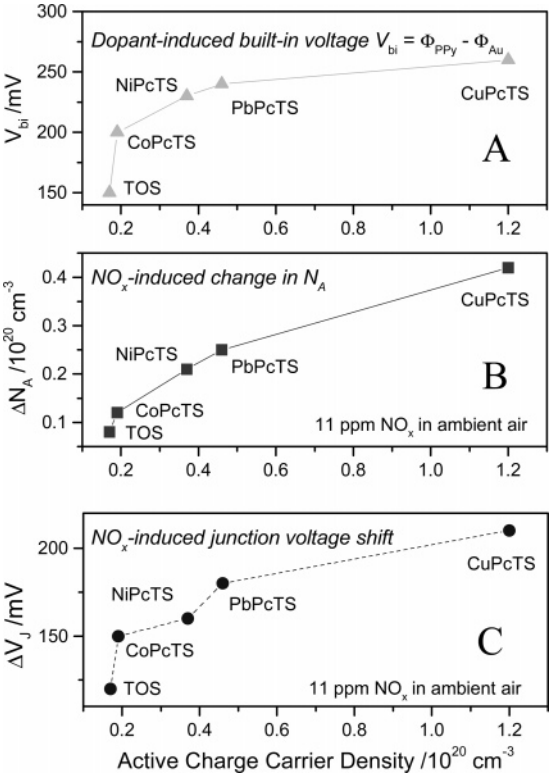

Figure 22. Dependence of the diode parameter and sensor response of Au/PPy-MPcTS Schottky barrier diodes on the nature of dopants.

to the effect of surface states and that the increase or decrease in the ideality factor may be due to a generation or reduction of the interface state density. Hence, the tendency of the ideality factor to decrease when the diode is exposed to NO_x may be attributed to the compensation of the interface states by NO_x molecules.[132]

In the low bias range, the diode current is primarily controlled by the depletion region and the gas response is usually explained in terms of the change of the work function (i.e., Fermi level) in the polymer layer. Capacitance−voltage ($C-V$) measurements show that PPy-CuPcTS exhibits the highest charge carrier density of all layers studied and hence the most positive work function. Hence, PPy-CuPcTS leads to the highest built-in voltage of all polymer diodes studied (Figure 22A). The interaction of PPy-CuPcTS with NO_2 causes the highest change in work function, which is related to the highest change in the charge carrier concentration, as $C-V$ measurements have shown (Figure 22B). Both effects are enhancing the sensor signal of the Schottky barrier diode when compared with work function measurements using Kelvin Probe or POSFET.[247] The charge carrier concentration of the PPy layer decreases from CuPcTS to TOS as dopant. The junction between PPy-TOS and Au shows a very low rectifying ratio due to the low built-in voltage and is practically quasi-ohmic. In this case, the bulk resistance cannot be neglected any more even in the low bias range. Hence, the tendency of the NO_2-induced junction voltage shift to decrease when the built-in voltage of the diode decreases can be explained in terms of the enhancement of the compensatory effect in the PPy bulk. This can be seen in Figure 22C along the series CuPcTS, PbPcTS, NiPcTS, CoPcTS, and TOS.

This effect is consistent with results obtained by Cabala et al.[121] They observed (1) an increase of the work function

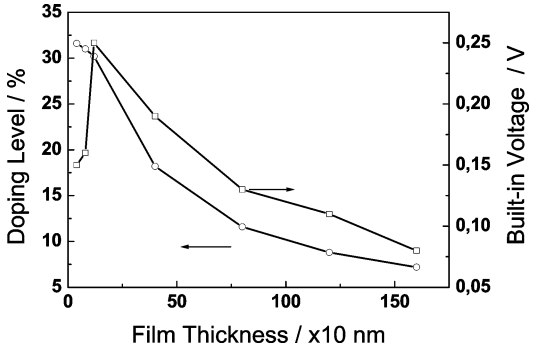

Figure 23. Doping level (○) and built-in voltage (□) as a function of PPy film thickness of Au/PPy-CuPcTS Schottky barrier diodes.

of doped PPy during exposure to NO_x, which was assumed to be due to an increase of the doping level, and (2) a decrease of the sensitivity toward NO_x from PPy-CuPcTS to PPy-PbPcTS and PPy-TOS.

According to the model given by Janata,[128] describing the chemical modulation of the work function of a sensitive polymer layer upon exposure to an interacting gas or vapor (see section 3.4.1), the magnitude and the polarity of the response depend on the value of the charge-transfer coefficient δ, with $|2\delta| < 1$ (eq 25). The charge-transfer coefficient δ can be estimated from quartz crystal microbalance (QCM) measurements during NO_x exposure. From the obtained data, an absorbed NO_x gas concentration of about 1.14×10^{20} cm^{-3} is deduced when the PPy layer is exposed to 11 ppm NO_x. Assuming that most absorbed NO_x molecules participate in the formation of a charge-transfer complex, a value of 0.36 can be deduced for the charge-transfer coefficient δ, taking into account the change of the charge carrier concentration in the PPy layer extracted from $C-V$ measurements ($N_A = 4.2 \times 10^{19}$ cm^{-3}). Evaluating the change in built-in voltage with NO_x gas concentration, a value of 0.41 is deduced for the charge-transfer coefficient δ. This value is slightly larger than that estimated from QCM measurements, and it indicates that the change in the Fermi level of PPy does not follow exactly the change in the charge carrier concentration according to eq 25 and eq 26, respectively. This fact may be attributed to the pinning of the Fermi level due to the presence of interface states, as discussed in section 3.3.3

Influence of Doping Level−Film Thickness. It is well-known that the doping level of MPcTS-doped PPy layers prepared by electropolymerization is strongly influenced by the PPy layer thickness. Rosenthal et al. have shown that the doping level of a MPcTS-doped PPy layer electrochemically formed at a constant potential decreases sharply when the PPy layer thickness increases.[248] The parasitic oxidation of the MPcTS dopant gives rise to a depletion layer near the electrode surface and, hence, to a decrease in the concentration of the dopant anions incorporated into the polymer backbone.

The influence of the film thickness on the doping level of PPy has been monitored *in situ* using EQCM measurements.[241,249] $J-V$ and $C-V$ measurements of Au/PPy-CuPcTS Schottky barrier diodes comprising PPy layers of different thicknesses showed that a decrease in the doping level causes a decrease in the Fermi level of PPy. As shown in Figure 23, the built-in voltage formed between the PPy layer and Au and, in turn, the depletion width of the junctions decrease according to eq 3.

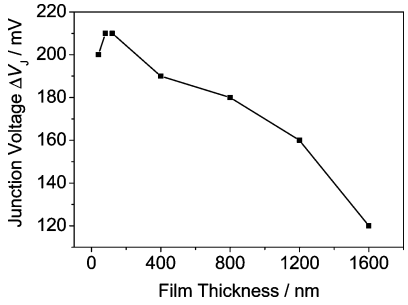

Figure 24. Change in junction voltage ΔV_J as a function of PPy film thickness of Au/PPy-CuPcTS Schottky barrier diodes.

The two compensatory effects of NO_x on the gas sensitivity of the Schottky barrier diodes in the bulk of PPy and at the interface region can be studied more extensively with the variation of the polymer film thickness, which strongly influences the doping level of the electropolymerized MPcTs-doped PPy layers.[248] They can be expressed as the changes in the junction and bulk voltages, which can be determined from the $J-V$ characteristics according to the following equations:

$$V_J \cong \frac{nkT}{e}\left(\ln \frac{J}{J_0}\right) \tag{43}$$

$$V_B = V_{bias} - V_J \tag{44}$$

The influence of the polymer film thickness of PPy-CuPcTS/Au diodes on chemical sensing properties, expressed as the change in the junction voltage ΔV_J upon exposure to NO_x, is shown in Figure 24. The NO_x-induced voltage shift ΔV_J, which was measured in the low bias range, decreases when the PPy film thickness increases. The increase in the bulk resistance due to the decrease of the doping level causes a stronger influence of the neutral bulk effect.

A decrease in the diode current exposed to NO_x is observed in the low bias voltage region, because the junction resistance R_J is dominant relative to the bulk resistance R_B. In the higher forward bias region, where the flat-band condition is reached, the depletion width W_J decreases to zero, the junction resistance reaches a minimum value, and the bulk resistance of the PPy layer may become dominant. Therefore, the gas response of the current−bias behavior is dominated by the gas-induced change of the PPy layer resistance.

Influence of Doping Level—Film Preparation Temperature. The effects of substrate temperature during film formation, of the annealing process on the film morphology and the crystalline structure, and the influence on the gas-sensing properties for NO_2 have been studied. Several authors have reported that, by manipulation of the film morphology, it is possible to control the sensitivity and response characteristics of the gas sensors.[198,250,251] Masui et al. found that the gas sensitivity of the amorphous copper phthalocyanine (CuPc) film is higher than that of the polycrystalline CuPc film because the amorphous film has a looser stacking of CuPc molecules and, hence, more adsorption sites for NO_x.[251]

Schottky barrier diodes based on PPy layers prepared at room temperature (295 K) do not show very large rectification ratios (Table 4). This may be due to a very thin barrier formed at Au/PPy junctions and may be an effect of the tunneling current.[137] With an acceptor concentration on the order of 10^{19} cm^{-3} and assuming the depletion width to scale as the square root of the acceptor density (eq 37), a depletion width of about 1−10 nm is expected for these devices. Hence, the tunneling current component cannot be neglected at room temperature (section 3.2.4). This is associated with the relatively large values of the ideality factor (see Table 4).

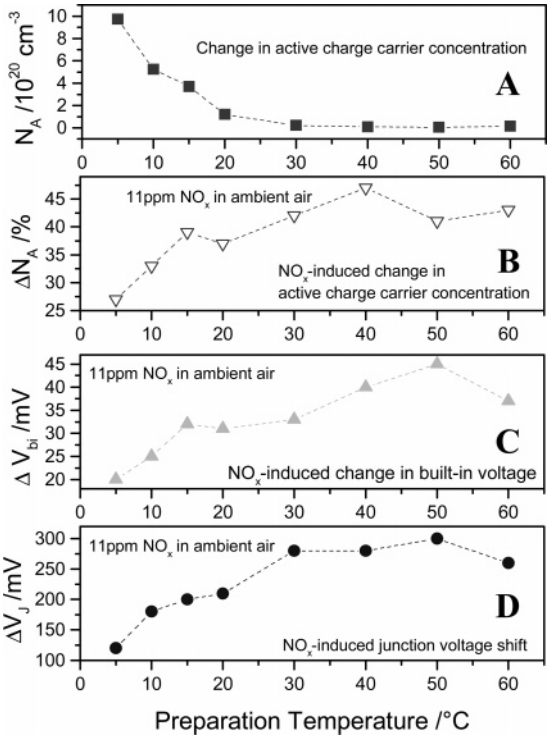

Figure 25. Dependence of the electrical parameter and sensor signal of a Au/PPy-CuPcTS Schottky barrier diode on the preparation temperature.

In general, the rectification ratio of diodes can be improved by the enhancement of the depletion width. According to eq 3, this may be reached either by increasing the built-in potential (i.e., contact potential) or by decreasing the active charge carrier concentration. It was found that the charge carrier concentration calculated from $1/C^2$ versus V curves is far different from that estimated from the doping level obtained from EQCM measurements.[241,249] ($\sim 10^{21}$ cm^{-3}), assuming that all dopant charges give rise to one hole polaron (or half a bipolaron). This may be due to the existence of a large concentration of defects in amorphous semiconductor materials. Due to these structural defects, the majority (about 80 to 90%) of the self-localized electronic defects (polarons or bipolarons) are trapped, such that they cannot contribute any more to the charge carrier transport through the polymer layer. The concentration of structural defects increases with increasing preparation temperature, because the polymerization rate rises simultaneously.[252]

In Figure 25 and Table 7 the electrical parameters of Au/PPy-CuPcTS Schottky barrier diodes can be found as a function of the polymerization temperature of PPy.[249] The rectification ratio increases rapidly with the increase of the preparation temperature, and simultaneously, the saturation current density decreases largely. This may be due to the enhancement of the defect concentration in PPy with the increase in the preparation temperature, which decreases the so-called active acceptor concentration and, hence, enhances the depletion width of the Schottky barrier according to eq 37.

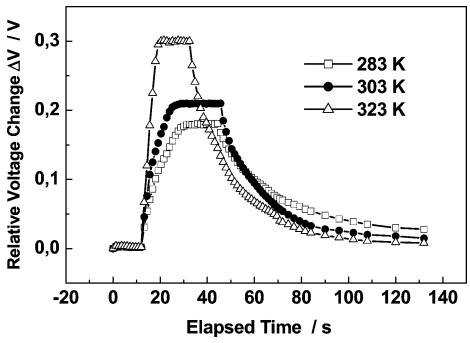

Figure 26. Transient response of a Au/PPy-CuPcTS Schottky barrier diode electrochemically prepared at different temperatures, exposed to 11 ppm NO_x in ambient air.

Therefore, the concentration of the active charge carriers is dependent on the preparation temperature and decreases with increasing preparation temperature (Figure 25A). Simultaneously, the size of the space charge region increases and therefore the junction resistance is enhanced with respect to the bulk resistance. Hence, the NO_2-induced shift of junction voltage increases for the same concentration (Figure 25D), enhancing the sensitivity of the Schottky barrier diode.

Furthermore, with increasing temperature, the crystallinity decreases and is zero when reaching the glass transition temperature (which is between 315 and 328 K for PPy-CuPcTS[64]). The gas or vapor can only be absorbed by the amorphous part of the polymer, which increases with the preparation temperature. Hence, NO_2 interacts more strongly with layers prepared at higher temperatures, leading to a higher relative change in the active charge carrier concentration (Figure 25B) and a higher change in the built-in voltage for the same NO_2 concentration (Figure 25C). Both effects cause a further increase of the gas-induced junction voltage shift with the preparation temperature.

The diffusion of gas or vapor in conducting polymers and their adsorption on polymer surfaces are the fundamental processes that control the chemical sensing response. It is supposed that diffusion processes in the crystalline polymer phase are much slower compared to those in the amorphous phase.[253] Hence, the polymerization temperature is an important parameter influencing the diffusion processes of polymeric sensor transducers. Figure 26 shows the response curves of diodes with PPy films exposed to 11 ppm NO_2. The diode based on the PPy film prepared at 323 K exhibits the response time and the recovery time, which are much faster than those of diodes based on PPy films prepared at 283 and 303 K. The decrease in response and recovery time can be explained by an increase in the amount of the amorphous phase compared to that of the crystalline phase in PPy when the preparation temperature increases.

5. Summary and Perspectives

Schottky barrier devices are promising candidates for sensor applications. The devices are simple to fabricate, obviating the need for expensive processes used in microtechnology. Both the metal and the semiconductor forming the Schottky barrier junction can be used as the chemical sensing components interacting with the gases or vapors. The material choices and combinations define the working principle, the sensitivity, and the selectivity of the sensor devices.

In Schottky barrier devices, particular attention must be paid to the formation of the junction barrier between the metal and the semiconductor. In the case of organic semiconductors, there is still only limited understanding of the interface between the organic material and the metal, which makes data interpretation complicated. Experimental data show that the junction barrier turns out to be not ideal because of the presence of interface states as well as the undesired formation of an interfacial layer caused either by instability of the components in air or by chemical reaction between the metals and semiconductors. The deviation from ideality can influence the sensor characteristics up to a complete breakdown of the ability to detect gases or vapors. Therefore, a high quality of the interface is the key factor affecting the sensing performances of the Schottky barrier devices. This certainly can increase the fabrication complexity and cost.

The key difference between organic and inorganic Schottky barrier junction devices is the ability of many gases and vapors to penetrate through the organic semiconductor to the interface either to change the Schottky junction resistance or to interact with the bulk of the semiconductor, which causes a work function change of the material. In the case of inorganic Schottky barrier junction devices, gas permeation toward the metal/semiconductor interface works only for hydrogen or hydrogen-producing compounds and causes formation of a dipole layer.

Organic semiconductors offer a viable alternative to conventional inorganic semiconductors for application in chemical sensors. They show sensitivities toward many gases or vapors, ranging from organic solvents to inorganic gases. Moreover, their porosity enables an ease of penetration of gases or vapors. The mechanical flexibility, environmental stability, and solution processability offer an enormous potential for applications within the field of microsensors. The macromolecular character and the high degree of flexibility in preparation make various physical and chemical properties realizable. The tunability of the sensing properties by the nature of the dopants as well as by the preparation procedures is an important benefit. Individual modification of each sensor is possible in only one step. This allows for the inexpensive fabrication of multisensing arrays, an aspect that makes sensors based on organic semiconductors suitable for commercialization. They are inherently compatible with solid-state integrated chemical sensors, because they can be readily incorporated into microfabricated structures. Additional benefits are the low device prices, the small dimensions, and low power consumption.

6. List of Symbols and Abbreviations

Δ	interfacial layer thickness, cm^2
δ	fractional charge-transfer coefficient upon gas interaction
ϵ_0	permittivity of free space, A s V^{-1} cm^{-1}
ϵ_s	permittivity of the semiconductor, A s V^{-1} cm^{-1}
ϵ_i	permittivity of the interfacial layer, A s V^{-1} cm^{-1}
ϕ_b	Schottky barrier height, eV
ϕ_e	effective barrier height, eV
$\Delta\phi_{bi}$	image force lowering of the barrier height, eV
ϕ_{bi}	contact potential or built-in potential, eV
$\mu_{p,n}$	charge carrier mobility, cm^2 V^{-1} s^{-1}
μ	dipole moment, A s cm^{-1}
θ	ratio of free to trapped charge carriers
τ	dielectric relaxation time, s
τ_{tr}	electron lifetime within the depletion layer, s

χ	electron affinity, eV
ω	angular frequency, Hz
ξ	energy difference between E_C and E_F, eV
A	area or junction area, cm^2
A^{**}	effective Richardson constant, A cm^{-2} K^{-2}
C	capacitance or capacity per area, F cm^{-2}
E	energy, eV
E_C	conduction band edge, eV
E_F	Fermi level, eV
E_{WF}	electron work function, eV
E_g	energy band gap, eV
E_{max}	maximum field strength at the metal/semiconductor interface, V cm^{-1}
E_V	valence band edge, eV
eV_0	band bending at zero applied voltage ($=\phi_{bi}$), eV
e	electronic charge, A s
h	Planck constant, J s
h_0	concentration of thermally generated holes in the valence band, cm^{-3}
J_0	saturation current density, A cm^{-2}
J	current density, A cm^{-2}
k	Boltzmann constant, J K^{-1}
L	layer thickness, cm
m^*	reduced mass of electron, kg
N_{ads}	density of adsorption sites, cm^{-3}
N_{ssb}	density of interface states, cm^{-2} eV^{-1}
N_C	effective density of states in the conduction band, cm^{-3}
N_D	donor concentration, cm^{-3}
N_{tr}	effective density of traps, cm^{-3}
N_V	effective density of state in the valence band, cm^{-3}
n	ideality factor
n_i	intrinsic electron concentration, cm^{-3}
p_{gas}	partial gas pressure, N m^{-2}
S	slope parameter
s	frequency exponent
T	absolute temperature, K
V	voltage or bias voltage at Schottky contact, V
V_{bi}	built-in voltage, V
V_d	diffusion voltage at zero bias voltage, V
V_r	reverse bias voltage, V
W	charge depletion zone or depletion layer width, cm
index "s"	semiconductor
index "m"	metal
index "h"	hole
index "e"	electron
index "b"	bulk
index "j"	junction
Alq_3	aluminum tris(8-hydroxychinoline)
BEDT-TTF	bis(ethylenedithio)tetrathiafulvalene
BN	benzonitrile
CELT	charging-energy-limited tunneling
CHEMFET	chemical sensitive field-effect transistor
DCM	dichloromethane
EQCM	electrochemical quartz crystal microbalance
F_4-TCNQ	tetrafluorotetracyanoquinodimethane
FIT	fluctuation-induced tunneling
HOMO	highest occupied molecular orbital
LUMO	lowest unoccupied molecular orbital
MIS	metal−insulator−semiconductor
MOSFET	metal-oxide-semiconductor field-effect transistor
MPcTS	metallophthalocyanine tetrasulfonate
OLED	organic light emitting diode
OFET	organic field-effect transistor
Pc	phthalocyanine
QCM	quartz crystal microbalance
THF	tetrahydrofuran
TPD	*N*,*N*′-diphenyl-*N*,*N*′-bis(3-methylphenyl)-1,1′-biphenyl-4,4′-diamine
VRH	variable-range hopping

7. References

(1) Göpel, W.; Hesse, J.; Zemel, J. N. *Sensors, A Comprehenisive Survey*; *Vol. 2, Chemical and Biochemical Sensors*; VCH Weinhein: New York, 1991.
(2) Janata, J. In *Solid-State Chemical Sensors*; Janata, J., Huber, R. J., Eds.; Academic Press: New York, 1985; and references therein.
(3) Lundström, I.; Shivaraman, M. S.; Svensson, C. M. *J. Appl. Phys. Lett.* **1975**, *46*, 3876.
(4) Janata, J.; Josowicz, M. *Nat. Mater.* **2003**, *2*, 19.
(5) Steele, M. C.; Hile, J. W.; Maclver, B. A. *J. Appl. Phys.* **1976**, *47*, 2537.
(6) Lundström, I.; Svensson, C. In *Solid State Chemical Sensors*; Janata, J., Huber, R. J., Eds.; Academic Press: New York, 1985; and references therein.
(7) Lechuga, L. M.; Calle, A.; Golmayo, D.; Tejedor, P.; Briones, F. *J. Electrochem. Soc.* **1991**, *138*, 159.
(8) Lechuga, L. M.; Calle, A.; Golmayo, D.; Briones, F. *Sens. Actuators, B* **1992**, *7*, 614.
(9) Liu, W. C.; Pan, H. J.; Chen, H. I.; Lin, K. W.; Cheng, S. Y.; Yu, K. H. *IEEE Trans. Electron Devices* **2001**, *48*, 1938.
(10) Yousuf, M.; Kuliyev, B.; Lalevic, B.; Poteat, T. L. *Solid-State Electron.* **1982**, *25*, 753.
(11) Kim, C. K.; Lee, J. H.; Lee, Y. H.; Cho, N. I.; Kim, D. J. *Sens. Actuators, B* **2000**, *66*, 116.
(12) Heeger, A. J. *Angew. Chem., Int. Ed.* **2001**, *40*, 2591.
(13) Burroughes, J. H.; Bradley, D. D. C.; Brown, A. R.; Marks, R. N.; MacKay, K.; Friend, R. H.; Burn, P. L.; Holmes, A. B. *Nature* **1990**, *347*, 539.
(14) Burn, P. L.; Holmes, A. B.; Kraft, A.; Bradley, D. D. C.; Brown, A. R.; Friend. R. H.; Gymer, R. W. *Nature* **1992**, *356*, 47.
(15) Alidiss, M., Ed. *Intrinsically Conducting Polymers: An Emerging Technology*; NATO ASI Series E; Kluwer: Dordrecht, 1993; Vol. 246.
(16) Sirringhaus, H.; Tessler, N.; Friend, R. H. *Science* **1998**, *280*, 1741.
(17) Wienk, M. M.; Kroon, J. M.; Verhees, J. H.; Knol, J.; Hummelen, J. C.; van Hal, P. A.; Janssen, R. A. J. *Angew. Chem., Int. Ed.* **2003**, *42*, 3371.
(18) Teh, K. S.; Lin, L. *J. Micromech. Microeng.* **2005**, *15*, 2019.
(19) Ho, P. K. H.; Thomas, D. S.; Friend, R. H.; Tessler, N. *Science* **1999**, *285*, 233.
(20) Pei, Q. B.; Yu, G.; Zhang, C.; Yang, Y.; Heeger, A. J. *Science* **1995**, *269*, 1086.
(21) Brabec, C. J.; Zerza, G.; Cerullo, G.; De Silvestri, S.; Luzzati, S.; Hummelen, J. C.; Sariciftci, N. S. *Chem. Phys. Lett.* **2001**, *340*, 232.
(22) Padinger, F.; Rittberger, R. S.; Sariciftci, N. S. *Adv. Funct. Mater.* **2001**, *11*, 1.
(23) Scheinert, S.; Paasch, G. *Phys. Status Solidi A* **2004**, *201*, 1263.
(24) Nishide, T.; Oyamada, T.; Akiyana, S.; Sasabe, H.; Adachi, C. *Adv. Mater.* **2006**, *18*, 3120.
(25) Bandyopadhyay, S.; Bhattacharyya, A.; Sen, S. K. *J. Appl. Phys.* **1999**, *85*, 3671.
(26) Janata, J. *Phys. Chem. Chem. Phys.* **2003**, *5*, 5155.
(27) Assadi, A.; Spetz, A.; Willander, M.; Svensson, C.; Lundström, I.; Inganäs, O. *Sens. Actuators, B* **1994**, *20*, 71.
(28) Miasik, J. J.; Hooper, A.; Tofield, B. C. *J. Chem. Soc., Faraday Trans.* **1986**, *82*, 1117.
(29) Tuyen, Le. T. T.; Potje-Kamloth, K.; Liess, H.-D. *Thin Solid Films* **1997**, *292*, 293.
(30) Hanawa, T.; Kuwabata, S.; Yoneyama, H. *J. Chem. Soc., Faraday Trans. 1*, **1988**, *84*, 1587.
(31) Ashcroft, N, W.; Mermin, N. D. *Solid State Physics*; Saunders: Philadelphia, 1976.
(32) Skotheim, T. A., Ed. *Handbook of Conducting Polymers, Vol. 1 and 2*; Marcel Dekker: New York, 1986.
(33) Arkhipov, V. I.; Heremans, P.; Emelianova, E. V.; Adriaenssens, G. J.; Bässler, H. *Appl. Phys. Lett.* **2003**, *82*, 3245.
(34) Tanase, C.; Blom, W. M.; de Leeuw, D. M.; Meijer, E. J. *Phys. Status Solidi* **2004**, *201*, 1236.
(35) Arkhipov, V. I.; Heremans, P.; Emeliannova, E. V.; Bässler, H. *Phys. Rev. B* **2005**, *71*, 055214.
(36) Koch, N.; Rajagopal, A.; Ghijsen, J.; Johnson, R. L.; Leising, G.; Pireaux, J.-J. *J. Phys. Chem. B* **2000**, *104*, 1434.
(37) Gao, W.; Kahn, A. *Org. Electron.* **2002**, *3*, 53.
(38) Shen, C.; Kahn, A.; Hill, I. G. In *Conjugated Polymer and Molecular Interfaces*; Salaneck, W. R., Seki, K., Kahn, A., Pireaux, J.-J., Eds.; Marcel Dekker: NewYork, 2001.
(39) Blochwitz, J.; Pfeiffer, M.; Fritz, T.; Leo, K.; Alloway, D. M.; Lee, P. A.; Armstrong, N. R. *Org. Electron.* **2001**, *2*, 97.
(40) Ganzorig, C.; Sugo, K.; Fujihira, M. *Mater. Sci. Eng., B* **2001**, *85*, 140.
(41) Ganzorig, C.; Fujihira, K. *Appl. Phys. Lett.* **2000**, *77*, 4211.

(42) Zhou, C.; Pfeiffer, M.; Blochwitz, J.; Werner, A.; Nollau, A.; Fritz, T.; Leo, K. *Appl. Phys. Lett.* **2001**, *78*, 410.
(43) Nollau, A.; Pfeiffer, M.; Fritz, T.; Leo, K. *J. Appl. Phys.* **2000**, *87*, 4340.
(44) Ritsko, J. J.; Fink, J.; Crecelius, G. *Solid State Commun.* **1983**, *46*, 477.
(45) Chance, R. R.; Boudreaux, D. S.; Bredas, J. L.; Silbey, R. In *Handbook of Conducting Polymers*; Skotheim, T. A., Ed.; Marcel Dekker: New York, 1986; Vol. 2, Chapter 24.
(46) Conwell, E. M. In *Organic Conductive Molecules and Polymers*; Nalwa, H. S., Ed.; John Wiley & Sons: Chichester, 1997; Vol. 4, Chapter 1.
(47) Heeger, A. J. In *Conjugated Polymers and Related Materials*; Salaneck, W. R., Lundström, I., Ranby, B., Eds.; Oxford Science Publications: Oxford, 1993; Chapter 4.
(48) Heeger, A. J.; Kivelson, S.; Schrieffer, J. R.; Su, W. P. *Rev. Mod. Phys.* **1988**, *60*, 781.
(49) Joo, J.; Long, S. M.; Pouget, J. P.; Oh, E. J.; MacDiarmid, A. G.; Epstein, A. J. *Phys. Rev. B* **1998**, *57*, 9567.
(50) Austin, I. A.; Mott, N. F. *Adv. Phys*. **1969**, *18*, 41.
(51) Elliot, S. R. *Philos. Mag*. **1971**, *36*, 1291.
(52) Mott N. F.; Davis, E. A. *Electronic Processes in Non-Crystalline Materials*; Clarendon-Press: Oxford, 1979.
(53) Sheng, P.; Abeles, B.; Arie, Y. *Phys. Rev. Lett.* **1973**, *31*, 44.
(54) Mott, N. F. *Metal-Insulator Transition*; Taylor-Francis: London, 1990; and references therein.
(55) Abeles, B.; Sheng, P.; Coutts, M. D.; Arie, Y. *Adv. Phys.* **1975**, 407.
(56) Joo, J.; Oblakowski, Z.; Du, G.; Pouget, J. P.; Oh, E. J.; Wiesinger, J. M.; Min, Y.; MacDiarmid, A. G. *Phys. Rev. B* **1994**, *49*, 2977.
(57) Pope, E:, Swenberg, C. E. *Electronic Processes in Organic Crystalls and Polymers*, 2nd ed.; Oxford University Press: Oxford, U.K., 1999.
(58) Bässler, H. *Phys. Status Solidi B* **1993**, *175*, 15.
(59) Dieckmann, A.; Bässler, H.; Borsenburger, P. M. *J. Chem. Phys.* **1993**, *99*, 8136.
(60) Novikov, S. V.; Vannikov, A. V. *J. Phys. Chem.* **1995**, *99*, 14573.
(61) Bässler, H. *Phys. Status Solidi B* **1993**, *175*, 15.
(62) Arkhipov, V. I.; Emelianova, E. V.; Adriaenssens, G. J. *Phys. Rev. B* **2001**, *63*, 081202(R).
(63) Mitchell, G.; Davis, F.; Legge, C. *Synth. Met*. **1988**, *26*, 247.
(64) Cabala, R. Ph.D. Thesis, Charles University, Prague, 1998.
(65) Epstein, A.; Rommelmann, H.; Bigelow, R.; Gibson, H.; Hoffmann, D.; Tanner, D. *Phys. Rev. Lett.* **1983**, *50*, 1866 and references therein.
(66) Pochtennyi, A. E.; Misevich, A. V. *Phys. Solid State* **1996**, *38*, 1422.
(67) Saunders, B. R.; Murray, K. S.; Fleming R. J.; Korbatich, Y. *Chem. Mater.* **1993**, *5*, 809 and references therein.
(68) Pfluger, P.; Weiser, G.; Scott, J. C.; Street, G. B. In *Handbook of Conducting Polymers*; Skotheim, T. A., Ed.; Marcel Dekker Inc.: New York, 1986; Vol. 2, Chapter 38.
(69) Anderson, W. *Commun. Solid State Phys.* **1970**, *2*, 193.
(70) Tenelsen, K.; Schreiber, M. *Phys. Rev. B* **1994**, *49*, 12662.
(71) Levy, Y. E.; Souillard, B. *Europhys. Lett.* **1987**, *4*, 233.
(72) Schreiber, M.; Grussbach, H. *Phys. Rev. Lett.* **1995**, *51*, 663.
(73) Sze, S. M.; Rhoderick, S. M.; Sharma, B. L.; Schottky, W. *Z. Phys*. **1939**, *113*, 367.
(74) Mott, N. F. *Proc. Cambridge Philos. Soc.* **1938**, *34*, 568.
(75) Sze, S. M.; Viturro, R.; Masilhiot, C.; Shaw, J. L.; Brillson, L. J.; LaGaffe, D.; Margaritondo, G.; Pettit, C. D.; Woodall, J. M. *J. Vac. Sci. Technol.* **1989**, *A7*, 855.
(76) Cowley, A. M.; Sze, S. M. *J. Appl. Phys.* **1965**, *36*, 3212.
(77) Rhoderick, E. H. *J. Appl. Phys.* **1975**, *46*, 2809.
(78) Braun, F. *Poggendorff's Ann. Phys.* **1874**, *153*, 556.
(79) Schottky, W. *Naturwissenschaften* **1938**, *26*, 843.
(80) Mott, N. F. *Proc. Cambridge Philos. Soc*. **1938**, *34*, 568.
(81) Sze, S. M. *Physics of Semiconductor Devices*; John Wiley & Sons: New York, 1981.
(82) Rhoderick, E. H.; Williams, R. H. *Metal-Semiconductor Contacts*; Oxford Science Publications: Oxford, U.K., 1988.
(83) Milnes, A. G.; Feucht, D. L. *Heterojunctions and Metal-Semiconductor Junctions*; Academic Press, Inc.: New York, 1972.
(84) Sadaoka, Y.; Jones, T. A.; Göpel, W. *J. Mater. Sci. Lett.* **1989**, *8*, 1095.
(85) Chen, H.; Rambhatla, A.; Janata, J.; Potje-Kamloth, K. *J. Electrochem. Soc.* **2007**, *154*, H354.
(86) Lampert, M. A.; Mark, P. *Current Injection in Solids*; Academic Press: New York, 1970.
(87) Crone, B. K.; Davids, P. S.; Campbell, I. H.; Smith, D. *J. Appl. Phys.* **1998**, *84*, 833.
(88) Karg, S.; Meier, M.; Riess. W. *J. Appl. Phys.* **1997**, *82*, 1951.
(89) Campbell, A. J.; Weaver, M. S.; Lidzey, D. G.; Bradley, D. D. *J. Appl. Phys.* **1998**, *84*, 6737.
(90) Crone, B. K.; Campbell, I. H.; Davids, P. S.; Smith, D. L. *J. Appl. Phys.* **1999**, *86*, 5767.
(91) Gustafsson, G.; Sundberg, M.; Inganäs, O.; Svensson, C. *J. Mol. Electron.* **1990**, *6*, 105.
(92) Townsend, P. D.; Friend, R. H. *Phys. Rev.* **1989**, *B40*, 3112.
(93) Henisch, H. K. *Semiconductor Contacts;* Clarendon: Oxford, U.K., 1984.
(94) Rhoderick, H. E.; Freeouf, J. L.; Woodall, J. M. *Appl. Phys. Lett.* **1981**, *39*, 72.
(95) Spicer, W. E.; Kendelewicz, T. J.; Newman, N.; Chin, K. K.; Lindau, I. *Surf. Sci.* **1986**, *168*, 240.
(96) Tersoff, J. *Phys. Rev. Lett.* **1984**, *52*, 476.
(97) Salaneck, W. R., Seki, K., Kahn, A., Pireaux. J. J., Eds. *Conjugated Polymer and Molecular Interfaces: Science and Technology for Photonic and Optoelectronic Applications*; Marcel Dekker: New York, 2002.
(98) Cahen, D.; Kahn, A.; Umbach, E. *Mater. Today* **2005**, *8*, 32.
(99) Ishii, H.; Sugiyama, K.; Ito, E.; Seki, K. *Adv. Mater.* **1999**, *11*, 605.
(100) Hill, I. G.; Rajagopal, A.; Kahn, A. *J. Appl. Phys.* **1998**, *84*, 3226.
(101) Mori, T.; Fujikawa, H.; Tokito, S.; Taga, Y. *Appl. Phys. Lett*. **1998**, *73*, 2763.
(102) Schlaf, R.; Parkinson, B. A.; Lee, P. A.; Nebesny, K. W.; Armstrong, N. R. *J. Phys. Chem. B* **1999**, *103*, 2984.
(103) Lee, S. T.; Wang, Y. M.; Hou, C. W.; Tang, C. W. *Appl. Phys. Lett.* **1999**, *74*, 670.
(104) Seki, K.; Nish, T.; Tanaka, S.; Komatsu, K.; Ikame, T.; Ishii, H.; Kanai, K. *Proc. Int. Symp. Super-Functionality Organic Devices*; IPAP Conf. Ser. 6; Institute of Pure and Applied Physics: Tokyo, 2005, p 178.
(105) Nishi, T.; Kanai, K.; Ouchi, Y.; Willis, M. R.; Seki, K. *Chem. Phys*. **2006**, *325*, 121.
(106) Salaneck, W. R., Seki, K., Kahn, A., Pireaux. J. J., Eds. *Conjugated Polymer and Molecular Interfaces: Science and Technology for Photonic and Optoelectronic Applications*; Marcel Dekker: New York, 2002.
(107) Yamane, H.; Yabuuchi, Y.; Fukagawa, H.; Kera, S.; Okudaira, K. K.; Ueno, U. *J. Appl. Phys.* **2006**, *99*, 093 705.
(108) Fukagawa, H.; Yamane, H.; Kataoka, T.; Kera, S.; Nakamura, M.; Kudo, K.; Ueno, N. *Phys. Rev. B: Condens. Matter Mater. Phys.* **2006**, *73*, 24531.
(109) Schroeder, P. G.; France, C. B.; Park, J. B.; Parkinson, B. A. *J. Appl. Phys.* **2002**, *91*, 3010.
(110) Morikawa, Y.; Ishii, H.; Seki, K. *Phys. Rev. B: Condens. Matter Mater. Phys.* **2004**, *69*, 041403.
(111) Witte, G.; Lukas, S.; Bagus, P. S.; Wöll, C. *Appl. Phys. Lett.* **2005**, *87*, 263502.
(112) Kahn, A.; Koch, N.; Gao, W. *J. Polym. Sci., Part. B: Polym. Phys*. **2003**, *41*, 2529.
(113) Gao, W.; Kahn, A. *J. Appl. Phys.* **2003**, *94*, 359.
(114) Kronik, L.; Shapira, Y. *Surf. Sci. Rep*. **1999**, *37*, 1.
(115) Heeger, A. J.; Parker, I. D.; Yang, Y. *Synth. Met.* **1994**, *67*, 23.
(116) Brazovskii, S.; Kirova, N. N. *Synth. Met.* **1993**, *55*−*57*, 1421.
(117) Davids, P. S.; Saxena, A.; Smith, D. L. *J. Appl. Phys.* **1995**, *78*, 4234.
(118) Dannetum, P.; Fahlman, M.; Fauquet, C.; Kaeijama, K.; Sononda, Y.; Lazzaroni, R. *Synth. Met.* **1994**, *6*, 133.
(119) Dannetum, P.; Lögland, M.; Salaneck, W. R.; Fredriksson, C.; Staftstöm, S.; Holmes, A. B.; Brown, A. R.; Graham, S.; Friend, R. H.; Lhost, O. *Mol. Cryst. Liq. Cryst.* **1993**, *43*, 228.
(120) Choong, V.; Park, Y.; Hsiejh, B. R.; Gao, Y. *J. Phys.* **1999**, *D30*, 1421.
(121) Cabala, R.; Meister, V.; Potje-Kamloth, K. *J. Chem. Soc., Faraday Trans.* **1997**, *93*, 131.
(122) Bott, B.; Thorpe, S. C. In *Techniques and Mechanism in Gas Sensing*; Moseley, P. T., Norris, J., Williams, D. E., Eds.; Adam Hilger Series on Sensors; IOP Publishing: Philadelphia, PA, 1991; Chapter 5.
(123) Van Ewyk, R. L.; Chadwick, A. V.; Wright, J. D. *J. Chem. Soc., Faraday Trans. 1* **1980**, *76*, 2194.
(124) Morrison, S. R. *The Chemical Physics of Surfaces*; Plenum Press: New York, 1977.
(125) Göpel, W. *Prog. Surf. Sci.* **1985**, *20*, 9.
(126) Blackwood, D.; Josowicz, M. *J. Phys. Chem.* **1991**, *95*, 493.
(127) Thieblemont, J. C.; Planche, V.; Petrescu, C.; Bouvier, J. M.; Bidan, G. *Polym. Degrad. Stab.* **1994**, *43*, 29.
(128) Janata, J. *Anal. Chem.* **1991**, *63*, 2546.
(129) Ruths, P.; Ashok, S.; Fonash, S.; Ruths, J. *IEEE Trans. Electron Devices* **1981**, *ED-28*, 1003.
(130) Johansson, M.; Lundström, I.; Ekedahl, L.-G. *J. Appl. Phys.* **1998**, *84*, 44.
(131) Card, H. C.; Rhoderick, E. H. *J. Phys. D: Appl. Phys.* **1971**, *4*, 1586.
(132) Nguyen, V. C.; Potje-Kamloth, K. *Thin Solid Films* **1999**, *338*, 142.
(133) Kanicki, J. In *Handbook of Conducting Polymers*; Skotheim, T. A., Ed.; Marcel Dekker Inc.: New York, 1986; Chapter 17.
(134) Chot, T. *Phys. Status Solidi A* **1981**, *66*, K43.
(135) Inganäs, O.; Skotheim, T.; Lundström, I. *J. Appl. Phys*. **1983**, *54*, 3636.

(136) Magaud, L.; Cyrot-Lackmann, F. *Encyclopedia of Applied Physics*; VCH: New York, 1996; Vol. 16.
(137) Bantikassegn, W.; Inganäs, O. *J. Phys. D: Appl. Phys.* **1996**, *29*, 2971.
(138) Macdonald, J. R.; Johnson, W. R. In *Impedance Spectroscopy*; Macdonald, J. R., Ed.; John Wiley & Sons, Inc.: New York, 1987.
(139) Lundström, I.; Shivaraman, M. S.; Svensson, S.; Lundkvist, I. *J. Appl. Phys. Lett.* **1975**, *26*, 55.
(140) Zhang, W.; de Vasconcelos, E. A.; Uchida, H.; Katsube, T.; Nakatsubo, T.; Nishioka, Y. *Sens. Actuators, B* **2000**, *65*, 154.
(141) Fang, Y. K.; Hwang, S. B.; Lin, C. Y.; Lee, C. C. *Appl. Phys. Lett.* **1990**, *57*, 2686.
(142) Tongson, L. L.; Knox, B. E.; Sullivan, T. E.; Fonash, S. J. *J. Appl. Phys.* **1979**, *50* 1535.
(143) Lundström, I. *Sens. Actuators, B* **1981/82**, *2*, 105.
(144) Tibuzzi, A.; Di Natale, C.; D'Amico, A.; Margesin, B.; Brida, S.; Zen, M.; Soncini, G. *Sens. Actuators, B* **2002**, *83*, 175.
(145) Rahimi, F.; Iraji Zad, A. *Sens. Actuators, B* **2006**, *115*, 164.
(146) Freeouf, J. L.; Woodhall, J. M. *Appl. Phys. Lett*. **1981**, *39*, 727.
(147) Cheng, S. Y. *Mater. Chem. Phys.* **2002**, *78*, 525.
(148) Cheng, C.-C.; Tsai, Y.-Y.; Kin, K.-W.; Chen, H.-I.; Hsu, W.-H.; Chuang, H.-M.; Chen, C.-Y.; Liu, W.-C. *Semicond. Sci. Technol.* **2004**, *19*, 778.
(149) Liu, W. C.; Pan, H. J.; Chen, H. I.; Lin, K. W.; Wang, C. K. *Jpn. J. Appl. Phys*. **2001**, *40*, 6254.
(150) Salehi, A.; Nikfarjam, A.; Jamshidi, D.; Kalantari, D. J. *Sens. Actuators, B* **2006**, *113*, 419.
(151) Salehi, A.; Kalantari, D. J. *Sens. Actuators, B* **2007**, *122*, 69.
(152) Chen, H.-I.; Chu, Y.-I. *Semicond. Sci. Technol.* **2004**, *19*, 39.
(153) Chen, H.-I.; Chou, Y.-I.; Hsiung, C.-K. *Sens. Actuators, B* **2003**, *92*, 6.
(154) Chen, H.-I.; Chou, Y.-I. *Semicond. Sci. Technol.* **2003**, *18*, 104.
(155) Talazac, L.; Barbain, F.; Varenne, C.; Mazet, L.; Pellier, S.; Soulier, C. *Sens. Actuators, B* **2002**, *83*, 149.
(156) Stutzmann, M.; Steinhoff, M.; Eickhoff, M.; Ambacher, O.; Nebel, C. E.; Schalwig, J.; Neuberger, R.; Müller, G. *Diamond Relat. Mater*. **2002**, *11*, 886.
(157) Hasegawa, H. *Curr. Appl. Phys.* **2007**, *7*, 318.
(158) Matsuo, K.; Hashizume, T.; Hasegawa, H. *Appl. Surf. Sci*. **2005**, *244*, 273.
(159) Hasegawa, H.; Oyama, S. *J. Vac. Sci. Technol., B* **2002**, *20*, 1647.
(160) Wang, H.; Chen, A.-B. *J. Appl. Phys*. **2000**, *87*, 7859.
(161) Ali, M.; Cimalla, V.; Lebedev, V.; Romanus, H.; Tilak, V.; Merfeld, D.; Sandvik, P.; Ambacher, O. *Sens. Actuators, B* **2006**, *113*, 797.
(162) Song, J.; Lu, W.; Flynn, J. S.; Brandes, G. R. *Solid-State Electron.* **2005**, *49*, 1330.
(163) Zhao, G.; Sutton, W.; Pavlidis, D.; Piner, E. L.; Schwank, J.; Hubbard, S. *IECE Trans. Electron.* **2003**, *E36-C*, 2027.
(164) Janson, M. S.; Linnarsson, M. K.; Hallén, A.; Svensson, B. G.; Achtziger, N.; Unéus, L.; Spetz, A. L.; Forsberg, U. *Phys. Scr*. **2004**, *T108*, 99.
(165) Kim, C K.; Lee, J. H.; Choi, S. M.; Noh, I. H.; Kim, H. R.; Cho, N. I.; Hong, C.; Jang, G. E. *Sens. Actuators, B* **2001**, *77*, 455.
(166) Hunter, G. W.; Neudeck, P. G.; Gray, M.; Androjna, D.; Chen, L.-Y.; Hoffman, R. W.; Liu, C. C.; Wu, Q. H. *Silicon Carbide, III-Nitride and Related Materials*; Transtech Publications: Switzerland, 2000; Vols. 338−342, p 1439.
(167) Chen, L.-Y.; Hunter, G. W.; Neudeck, P. G.; Knight, D. *Solid-State Electron.* **1998**, *42*, 2209.
(168) Zubkans, J.; Spetz, A. L.; Sundgren, H.; Winquist, F.; Kleperis, J.; Lusis, A.; Lundström, I. *Proc. 8th Int. Conf. Solid-State Sens. Actuators, Technical Digest*, Vol. 1, Stockholm, Sweden, IEEE: New York, 1995; p 726.
(169) Wenyi, Z.; Vasconcelos, E. A.; Uchida, H.; Katsube, T.; Nakatsubo, T.; Nishioka, Y. *Sens. Actuators, B* **2000**, *65*, 154.
(170) Khan, S. A.; Vasconcelos, E. A.; Uchida, E. A.; Katsube, T. *Sens. Actuators, B* **2003**, *92*, 181.
(171) Hollingsworth, R. E.; Sites, J. R. *J. Appl. Phys*. **1982**, *53*, 6367 and references therein.
(172) Hobeon, W. S.; Ellis, A. B. *J. Appl. Phys.* **1983**, *54*, 6956 and references therein.
(173) Carpenter, M. K.; Van Ryswyk, H. V.; Ellis, A. B. *Langmuir* **1985**, *1*, 605.
(174) Bailey, R. A.; Persaud, K. C. In *Polymer Sensors and Actuators*; Osada, Y., De Rossi, D. E., Eds.; Springer-Verlag: Berlin, 2000.
(175) Liang, W. L.; Lei, J.; Martin, Ch. R. *Synth. Met.* **1992**, *52*, 227.
(176) Riad, A. S. *Physica B* **1999**, *270*, 148.
(177) Hiramoto, M. *Jpn. J. Appl. Phys*. **2003**, *42*, 672.
(178) Parker, I. D. *J. Appl. Phys*. **1994**, *75*, 1656.
(179) Wang, H. L.; MacDiarmid, A. G.; Wang, Y. Z.; Gebler, D.; Epstein, A. J. *Synth. Met*. **1996**, *78*, 33.
(180) Singh, R.; Narula, A. K.; Tandon, R. P.; Mansingh, A.; Chandra, S. *J. Appl. Phys.* **1996**, *79*, 1476.
(181) Bantikassegn, W.; Dannetun, P.; Inganäs, O.; Salaneck, W. R. *Thin Solid Films* **1993**, *224*, 232.
(182) Koezuka, H.; Etoh, S. *J. Appl. Phys*. **1983**, *54*, 2511.
(183) Bantikassegn, W.; Dannetun, P.; Inganäs O.; Salaneck, W. R. *Synth. Met*. **1993**, *55*−*57*, 36.
(184) Glenis, S.; Tourillon, G.; Garnier, F. *Thin Solid Films* **1986**, *139*, 221.
(185) Singh, R.; Narula, A. K. *Appl. Phys. Lett.* **1997**, *71*, 2845.
(186) Nguyen, V. C. Ph.D. Thesis, Universität der Bundeswehr München, 2000.
(187) Gould, R. D. *Coord. Chem. Rev*. **1996**, *156*, 237.
(188) Fujii, A.; Ohmori, Y.; Yoshino, K. *IEEE Trans. Electron. Devices* **1997**, *44*, 1204.
(189) Law, K. Y. *Chem. Rev.* **1993**, *93*, 439.
(190) Guillaud, G.; Simon, J.; Gewain, J. P. *Coord. Chem. Rev*. **1998**, *178*−*80*, 1433.
(191) Gould, R. D.; Shafai, T. S. *Superficies Vacio* **1999**, *9*, 226.
(192) Riad, A. S. *Physica B* **1999**, *270*, 148.
(193) Rajesh, K. R.; Menon, C. S. *Can. J. Phys*. **2005**, *83*, 1151.
(194) Samuel, M.; Menon, C. S.; Umnikrishnan, N. V. *Semicond. Sci. Technol*. **2006**, *21*, 677.
(195) Brown, A. R.; Bradley, D. D. C.; Burroughes, J. H.; Friend, R. H.; Greenham, N. C.; Burn, P. L.; Holmes, A. B.; Kraft, A. *Appl. Phys. Lett.* **1992**, *61*, 2793.
(196) Sharma, G. D. *Synth. Met.* **1995**, *74*, 227.
(197) Honeybourne, C. L.; Ewen, R. J. *J. Phys. Chem. Solids* **1983**, *44*, 833.
(198) Sadaoka, A.; Jones, T. A.; Göpel, W. *Sens. Actuators, B* **1990**, *1*, 148.
(199) Gould, R. D.; Ibrahim, N. A. *Thin Solid Films* **2001**, *398*−*399*, 432.
(200) Wang, H. Y.; Ko, W. H.; Batzel, D. A.; Kenney, M. E.; Lando, J. B. *Sens. Actuators, B* **1990**, *1*, 1138.
(201) Schoch, K. F.; Temofonte, T. A. *Thin Solid Fillms* **1988**, *165*, 83.
(202) Nieuwenhiuzen, M. S.; Nederlof, A. J.; Barendsz, A. W. *Anal. Chem*. **1988**, *60*, 230.
(203) Musa, I.; Eccleston, W. *Jpn. J. Appl. Phys.* **1998**, *37*, 4288.
(204) Assadi, A.; Fu, Y.; Willander, M.; Svensson, C. *Jpn. J. Appl. Phys.* **1993**, *32*, 1696.
(205) Fang, Y.; Chen, S.-A. *Mater. Chem. Phys.* **1992**, *32*, 380.
(206) Jen, K. Y.; Miller, G. G.; Elsenbaumer, R. L. *J. Chem. Soc., Chem. Commun.* **1986**, 1346.
(207) Garnier, F.; Yassar, R.; Hajlaoui, R.; Horowitz, G.; Deloffre, F.; Servet, B.; Ries, S.; Alnot, P. *J. Am. Chem. Soc*. **1993**, *115*, 8716.
(208) Greenham, N. C.; Moratt, S. C.; Bradley, D. D.; Friend, R. H.; Homes, A. B. *Nature* **1993**, *365*, 628.
(209) Chittibabu, K. G.; Kamath, M.; Kumar, J.; Tripathy, S. K. *Chem. Mater*. **1994**, *6*, 475.
(210) Sundberg, M.; Gustafsson, G.; Inganäs, O. *Appl. Phys. Lett.* **1990**, *57*, 733.
(211) Turut, A.; Köleli, F. *J. Appl. Phys.* **1992**, *72*, 818.
(212) Kuo, C. S.; Wakim, F. G.; Sengupta, S. K.; Tripathy, S. K. *Jpn. J. Appl. Phys.* **1994**, *33*, 2629.
(213) Lous, E. J.; Blom, P. W. M.; Molenkamp, L. W.; de Leeuw, D. M. *Phys. Rev. B* **1995**, *51*, 17251.
(214) Musa, I.; Eccleston, W. *Jpn. J. Appl. Phys.* **1998**, *37*, 4288.
(215) Abdou, M. S. A.; Orfino, P.; Xie, Z. W.; Deen, M.; Holderoft, S. *Adv. Mater*. **1994**, *6*, 838.
(216) Tagmouti, S.; Oueriagli, A.; Outzourhit, A.; Khaidar, M.; Ameziane, El. L.; Yassar, A.; Youssioufi, H. K.; Garnier, F. *Synth. Met.* **1997**, *88*, 109.
(217) Ohmori, Y.; Takahashi, H.; Kawai, T.; Yoshino, K. *J. Appl. Phys*. **1990**, *29*, L1849.
(218) Triverdi, D. C. In *Organic Conductive Molecules and Polymers*; Nalwa, H. S., Ed.; John Wiley & Sons: Chichester, U.K., 1997; Vol. 2.
(219) Green, A. G.; Woodhead, A. E. *J. Chem. Soc. Trans.* **1910**, *97*, 2388.
(220) Chen, S.-A.; Fang, Y. *Synth. Met.* **1993**, *60*, 215.
(221) Gupta, R. K.; Singh, R. A. *Comput. Sci. Technol.* **2005**, *65*, 677.
(222) Yang, C.-H. *J. Electrochem. Soc.* **1999**, *146*, 1939.
(223) Abthagir, P. S.; Saraswathi, R. *J. Mater. Sci.: Mater. Electron*. **2004**, *15*, 81.
(224) Calderone, A.; Lazzaroni, R.; Bredas, J. L. *Synth. Met.* **1993**, *55*−*57*, 4620.
(225) Wu, S.; Zeng, F.; Li, F.; Zhu, Y. *Eur. Polym. J.* **2000**, *4*, 679.
(226) Li, J.; Petelenz, D.; Janata, J. *Electroanalysis* **1993**, *5*, 791.
(227) Conn, C.; Sestak, S.; Baker, A. T.; Unsworth, J. *Electroanalysis* **1998**, *10*, 1137.
(228) Campos, M.; Bulhoes, L. O. S.; Lindino, C. A. *Sens. Actuators, A* **2000**, *87*, 67.
(229) Rodríguez, J.; Grande, H.; Otero, T. In *Organic Conductive Molecules and Polymers*; Nalwa, H. S., Ed.; John Wiley & Sons: Chichester, England, 1997; Vol. 2 and references therein.
(230) Warren, F. L.; Anderson, P. *J. Electrochem. Soc.* **1987**, *134*, 101.

(231) Saunders, B. R.; Fleming, R. J.; Murray, K. S. *Chem. Mater*. **1995**, *7*, 1082.
(232) Walton, D. J.; Hall, C. E.; Chyla, A.; Viney I. V. F.; Mure, J.-M. *Synth. Met.* **1993**, *55*−*57*, 1465.
(233) Gupta, R.; Misra, K. C.; Malhotra, B. D.; Beladakere, N. N.; Chandra, S. *Appl. Phys. Lett.* **1991**, *58*, 51.
(234) Kanazawa, K. K.; Diaz, A. F.; Kronubi, M. T.; Street, G. B. *Synth. Met.* **1981**, *4*, 119.
(235) Inganäs, O.; Lundström, I. *Synth. Met.* **1984/5**, *10*, 5.
(236) Dhawan, S. K.; Triverdi, D. C. *Synth. Met.* **1993**, *60*, 67.
(237) Green, M. A.; King, F. D.; Shewchun, J. *Solid-State Electron.* **1974**, *17*, 55.
(238) Ohmori, Y.; Takahashi, H.; Muro, K.; Uchida, M.; Kawai, T.; Yoshino, K. *Jpn. J. Appl. Phys., Part 2* **1991**, *30*, L1247.
(239) Taylor, D. M.; Gomes, H. L. *J. Phys. D: Appl. Phys.* **1995**, *28*, 2554.
(240) Gupta, R. *Appl. Phys. Lett.* **1991**, *58*, 51.
(241) Topart, P.; Josowicz, M. *J. Phys. Chem.* **1992**, *96*, 7824.
(242) Buhks, E.; Hodge, I. M. *J. Chem. Phys.* **1983**, *11*, 5976.
(243) Nagase, H.; Wakabayashi, K.; Imanka, T. *Sens. Actuators, B* **1993**, *13*−*14*, 596.
(244) Topart, P.; Josowicz, M. *J. Phys. Chem.* **1992**, *96*, 7824.
(245) Barisci, J. N.; Wallace, G. G.; Andrews, M. K.; Partridge, A. C.; Harris, P. D. *Sens. Actuators, B* **2002**, *84*, 252.
(246) Bardeen, J. *Phys. Rev.* **1947**, *71*, 717.
(247) Potje-Kamloth, K. *Crit. Rev. Anal. Chem.* **2002**, *32*, 121.
(248) Rosenthal, M. V.; Skotheim, T. A.; Linkous, C. A. *Synth. Met.* **1986**, *15*, 219.
(249) Nguyen, V. C.; Potje-Kamloth, K. *J. Phys. D: Appl. Phys.* **2000**, *33*, 1.
(250) Lee, Y.-L.; Tsai, W.-C.; Maa, J.-R. *Appl. Surf. Sci*. **2001**, *173*, 352.
(251) Masui, M.; Sasahara, M.; Wada, T.; Takeuchi, M. *Appl. Surf. Sci*. **1996**, *92*, 643.
(252) Novak, P. *Electrochim. Acta* **1992**, *37*, 1227.
(253) Hsieh, J. C.; Liu, C. J.; Ju, Y. H. *Thin Solid Films* **1998**, *322*, 98.

CR0681086